iScience

CellPress
OPEN ACCESS

Article

Vascular endothelial cells-derived exosomes synergize with curcumin to prevent osteoporosis development

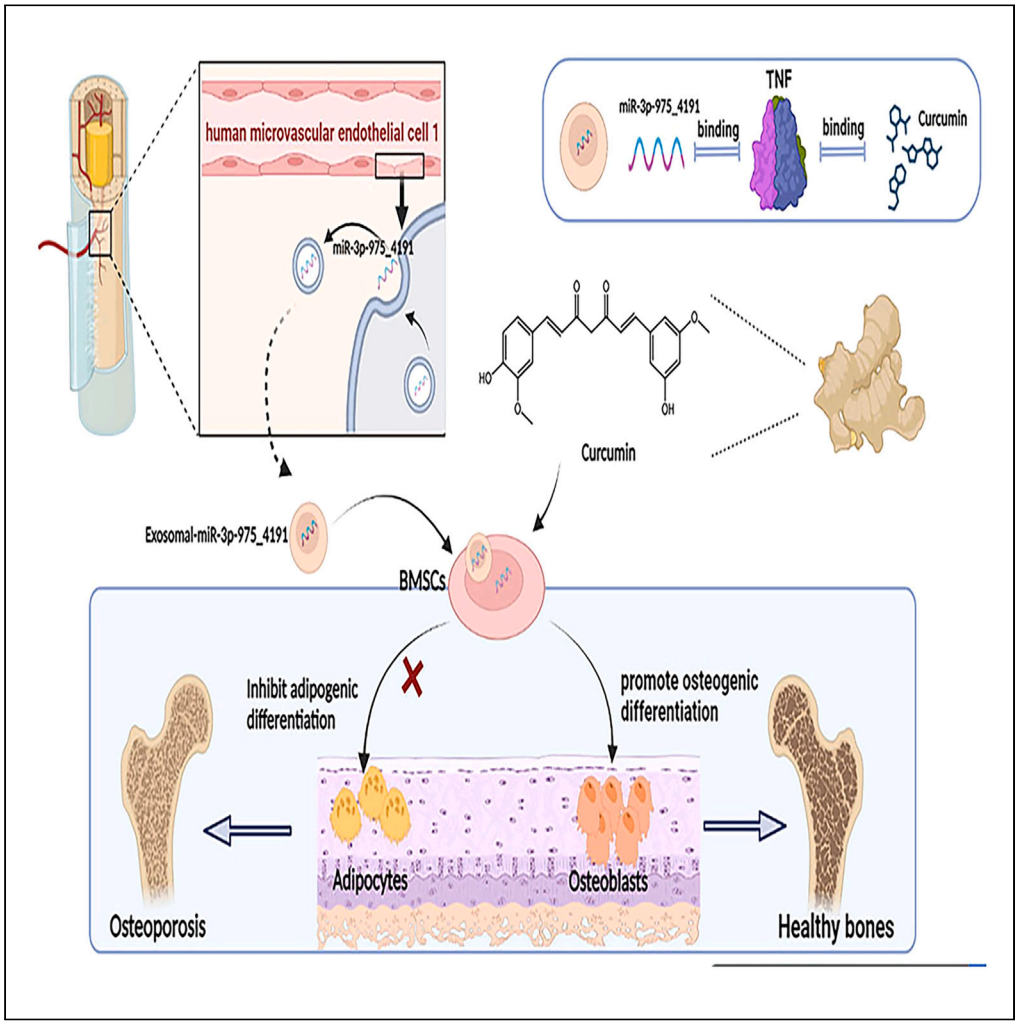

Jiaojiao Wang, Xinyan Xie, Hang Li, ..., Yajun Chen, Jieyu He, Qiong Lu

christy_luq@csu.edu.cn

Highlights

EC-EXOs play a key role in regulating BMSCs differentiation through miR-3p-975_4191

MiR-3p-975_4191 regulates the differentiation of BMSCs through inhibition of TNF

EC-EXOs may act synergistically with curcumin to delay the process of osteoporosis

Wang et al., iScience 27, 109608
April 19, 2024
https://doi.org/10.1016/j.isci.2024.109608

iScience

CellPress
OPEN ACCESS

Article

Vascular endothelial cells-derived exosomes synergize with curcumin to prevent osteoporosis development

Jiaojiao Wang,[1,2] Xinyan Xie,[1,3] Hang Li,[1,2] Qiyue Zheng,[1,2] Yun Chen,[1,2] Wenjie Chen,[1,2] Yajun Chen,[1,2] Jieyu He,[4] and Qiong Lu[1,2,5,*]

SUMMARY

Osteoporosis has gradually become a major public health problem. Further elucidation of the pathophysiological mechanisms that induce osteoporosis and identification of more effective therapeutic targets will have important clinical significance. Experiments *in vitro* on bone marrow stem cells (BMSCs) subjected to osteogenic and adipogenic differentiation and *in vivo* on surgical bilateral ovariectomy (OVX) mouse models revealed that exosomes of vascular endothelial cells (EC-EXOs) can promote osteogenic differentiation of BMSCs and inhibit BMSC adipogenic differentiation through miR-3p-975_4191. Both miR-3p-975_4191 and curcumin can target tumor necrosis factor (TNF) and act synergistically to regulate BMSCs fate differentiation and delay the progression of osteoporosis. Our findings suggest that EC-EXOs may exert a synergistic effect with curcumin in reversing the progression of osteoporosis by targeting TNF via miR-3p-975_4191. Our study may provide therapeutic options and potential therapeutic targets for osteoporosis and thus has important clinical implications.

INTRODUCTION

Osteoporosis is a disease characterized by low bone mass and deterioration of the microarchitecture and mechanical properties of bone tissue.[1] Enhanced adipogenic differentiation and reduced osteogenic differentiation of bone marrow stem cells (BMSCs) in the bone marrow are major causes of osteoporosis.[2] Bone is a highly vascularized tissue, and the close spatial and temporal connection between bone and angiogenesis is known as angiogenic-osteogenesis coupling.[3] Vascular endothelial cells (ECs) play essential roles in the biological processes that couple vascular and osteogenic mechanisms and thus help to regulate the proliferation and differentiation of BMSCs. Vascular ECs are themselves regulated by the secretory proteins vasoactive endothelial growth factor (VEGF), platelet-derived growth factor beta polypeptide (PDGF-β), and semaphorin3 (SLIT3) and signaling pathways such as the hypoxia inducible factor-1 (HIF 1α), and Notch pathways.[3–5] Overall, growth factors and pathways in osteoblasts, osteoclasts, and vascular ECs control the interaction between osteogenesis and angiogenesis.

Exosomes are a class of paracrine factors that are regarded as important tools for cell-cell communication.[6] Exosomes target specific cells or tissues, and they can deliver short interfering RNAs, antisense oligonucleotides, chemotherapeutic agents, and immunomodulators to their desired targets for the treatment of various diseases.[7,8] Whether human vascular endothelial cell-derived exosomes (EC-EXOs) can regulate the osteogenic-adipogenic fate differentiation of BMSCs and the related mechanisms have not yet been reported. In the current study, based on the existing evidence regarding vascular ECs and exosomes, we investigated the mechanisms by which EC-EXOs regulate the osteogenic-adipogenic fate differentiation of BMSCs via miRNA in osteoporosis.

Combined treatment with exosomes and drugs may become an effective strategy to treat diseases. In our study, miR-3p-975_4191 was found to act on tumor necrosis factor (TNF), and bioinformatics analysis revealed that curcumin also acted on TNF. We therefore combined exosomes with curcumin. Compared with drugs used in the clinical treatment of osteoporosis, the active ingredients of Chinese medicines have the advantages of low cost and safety without side effects. Curcumin is a natural polyphenolic compound derived from turmeric.[9] Previous studies by our group have confirmed the effect of curcumin in promoting the osteogenic differentiation of BMSCs.[10] Therefore, in this study, we further explored whether EC-EXOs can act synergistically with curcumin to regulate the fate differentiation of BMSCs. Targeting this fundamental mechanism to prevent bone aging may be an effective therapeutic strategy not only for osteoporosis but also for various age-related diseases.

[1]Department of Pharmacy, The Second Xiangya Hospital, Central South University, Changsha, Hunan 410011, P.R. China
[2]Institute of Clinical Pharmacy, Central South University, Changsha, Hunan 410011, P.R. China
[3]Mathematical Engineering Academy of Chinese Medicine, Guangzhou University of Chinese Medicine, Guangzhou, Guangdong 510006, P.R. China
[4]Department of Geriatrics, The Second Xiangya Hospital of Central South University, 139 Middle Renmin Road, Changsha, Hunan 410011, P.R. China
[5]Lead contact
*Correspondence: christy_luq@csu.edu.cn
https://doi.org/10.1016/j.isci.2024.109608

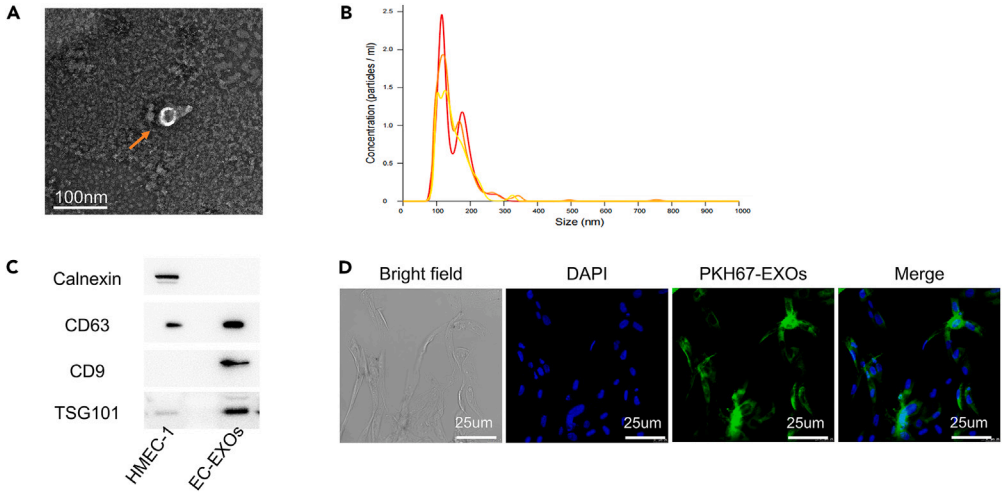

Figure 1. Characterization of exosomes derived from HMEC-1 cells

(A) EC-EXOs observed by transmission electron microscopy (scale bar: 100 nm).

(B) The particle sizes of exosomes were analyzed.

(C) Western blotting was performed to detect the expression of the exosomal markers CD63, CD9 and TSG101.

(D) The internalization of PKH26-labeled exosomes by BMSCs was observed under a fluorescence microscope.

RESULTS

Isolation and identification of EC-EXOs from HMEC-1 cells

EC-EXOs were isolated by ultracentrifugation and photographed with transmission electron microscopy (TEM). Some round or oval vesicles with a double-membrane structure and uniform size were visible (Figure 1A). The average particle size of EC-EXOs was 148.9 nm, as shown by nanoparticle tracking analysis (NTA), and most of the exosomes were in the size range of 30~200 nm (Figure 1B). Western blot analysis showed that the EC-EXOs expressed exosome-specific positive protein markers, including calnexin, CD63, CD9, and TSG101 (Figure 1C). Next, we tested whether EC-EXOs could be absorbed by BMSCs. EC-EXOs were labeled with the fluorescent dye PKH26 and added to BMSC culture medium. Laser confocal microscopy showed that PKH67-labeled exosomes were absorbed by BMSCs (Figure 1D).

EC-EXOs promote osteogenic differentiation of BMSCs

Next, we investigated whether EC-EXOs affect the osteogenic differentiation of BMSCs *in vitro*. BMSCs were treated with different concentrations of EC-EXOs (0 μg/mL, 25 μg/mL, 50 μg/mL, and 100 μg/mL). The different groups of BMSCs were continuously cultured with osteogenic induction medium for 21 days and then stained with Alizarin red S dye. The results showed that EC-EXOs promoted calcium nodule formation in BMSCs in a concentration-dependent manner (Figures 2A and 2B). To further confirm the effect of EC-EXOs on the osteogenic differentiation of BMSCs, we tested the expression of the osteogenic-related genes OPN, RUNX2, osteocalcin (OCN), and OC in BMSCs after treatment with EC-EXOs for 7 days by RT-qPCR analysis. OPN, RUNX2, OCN, and OC mRNA levels were significantly increased in the EC-EXO group compared to the control group (Figures 2C–2G). These results indicate that EC-EXOs can induce osteogenic differentiation of BMSCs *in vitro*.

EC-EXOs inhibit adipogenic differentiation of BMSCs

BMSCs are a group of pluripotent stem cells with osteogenic or adipogenic differentiation potential. To investigate the effect of EC-EXOs on the adipogenic differentiation of BMSCs, we treated BMSCs with different concentrations of EC-EXOs (0 μg/mL, 25 μg/mL, 50 μg/mL, and 100 μg/mL). The different groups of BMSCs were continuously cultured with adipogenic induction medium for 14 days and stained with Oil red O. The results showed that EC-EXOs inhibited lipid droplet formation in a concentration-dependent manner (Figures 2H and 2I). The effect of EC-EXOs on the adipogenic differentiation of BMSCs was further verified by RT-qPCR, which showed that EC-EXO treatment significantly reduced the expression of adipogenic differentiation-related genes, including Pparg, CD36, and Cebpα (Figures 2J–2L). What's more, we induced osteoclast precursor Raw264.7 cells using macrophage colony-stimulating factor (M-CSF) and receptor activator of nuclear factor kappa-B ligand (RANKL), and simultaneously treated with PBS and EC-EXOs. qPCR results showed that EC-EXOs could significantly downregulate the expression of osteoclast-related genes c-Fos and NFATc1 (Figure S1). These results demonstrate that EC-EXOs significantly inhibit the adipogenic differentiation of BMSCs.

EC-EXOs increase bone formation and reduce bone marrow fat accumulation in aged mice

To explore whether EC-EXOs affect bone formation, we injected 15-month-old mice with EC-EXOs (150 μg/100ul) three times a week by tail vein. One month after injection, the femurs were collected and scanned by a micro-CT system. Both 2D and 3D maps of Micro-CT analysis

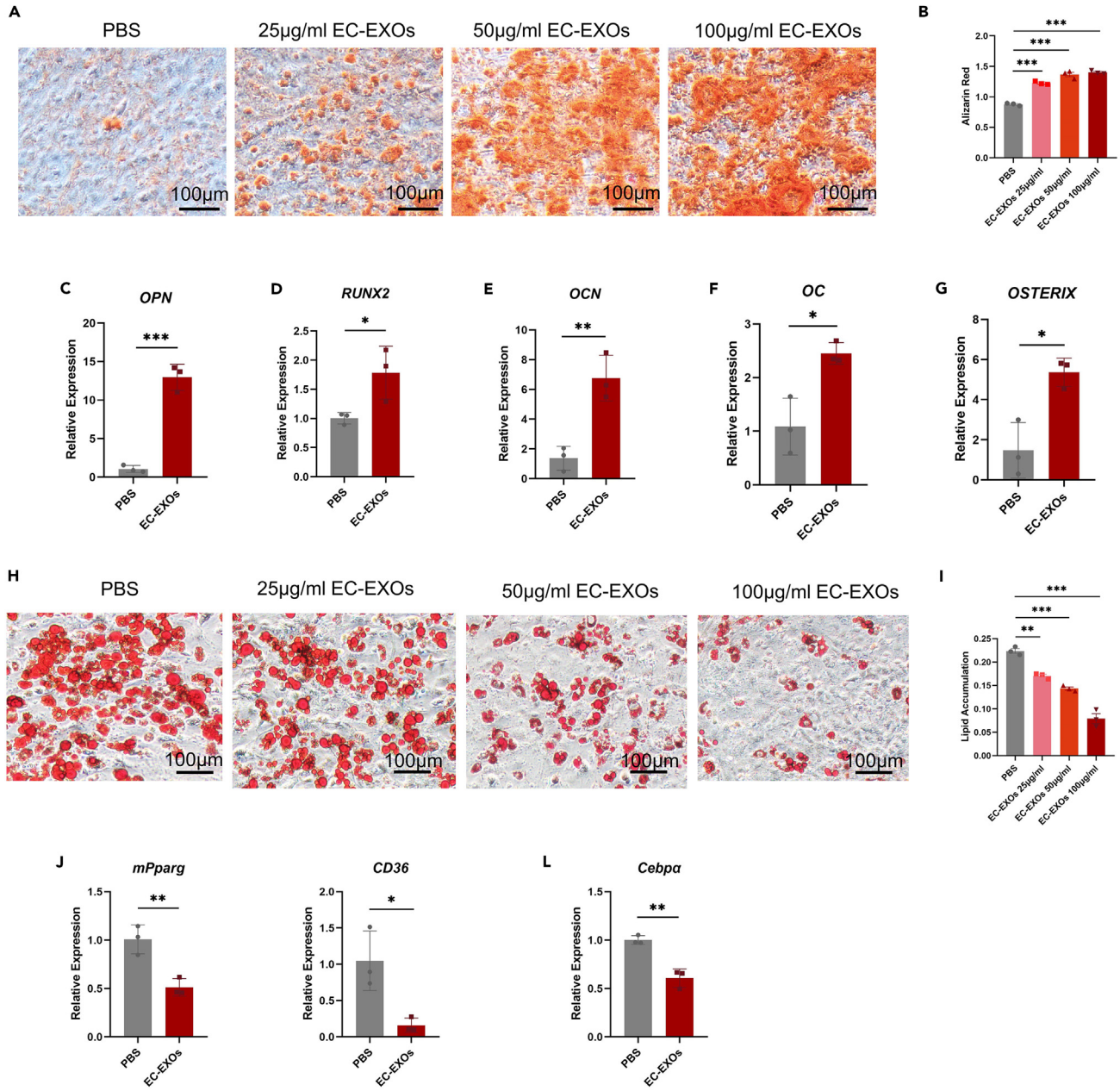

Figure 2. EC-EXOs can promote osteogenic differentiation and inhibit adipogenic differentiation of BMSCs

(A) Representative images of Alizarin red staining after 21 days of osteogenic induction and (B) quantification of calcification of BMSCs among different groups. Scale bar, 100 μm.

(C–G) The mRNA expression levels of osteogenic biomarkers (OPN, RUNX2, OCN, OC, and OSTERIX) in osteogenically differentiated BMSCs in different groups on Day 7 were detected by RT-qPCR.

(H) Oil red O staining and (I) quantification of BMSCs among the different groups after adipogenic induction for 14 days. Scale bar, 100 μm.

(J–L) The mRNA expression levels of adipogenic biomarkers (mPparg, CD36, and Cebpα) in adipogenically differentiated BMSCs in different groups on Day 7 were detected by RT-qPCR. β-Actin was used as an internal control. The values were expressed as mean ± SEM, *p < 0.05, **p < 0.01, ***p < 0.001.

showed that EC-EXOs promoted bone formation in aged mice (Figures 3A and 3B). Osteometric parameter analysis showed that EC-EXOs increased bone volume (BV/TV) and trabecular thickness (Tb.Th) but had no effect on trabecular number (Tb.N) and trabecular separation (Tb.Sp) (Figures 3C–3F). HE staining showed that EC-EXO treatment caused no damage to various organs, including the heart, liver, spleen, lungs, and kidneys, in aged mice with slowed metabolism (Figure 3G). The physiological condition of all organs was normal, and the biocompatibility of EC-EXOs was not abnormal in aged mice. HE staining showed that there were significantly fewer fat vacuoles in the bone marrow

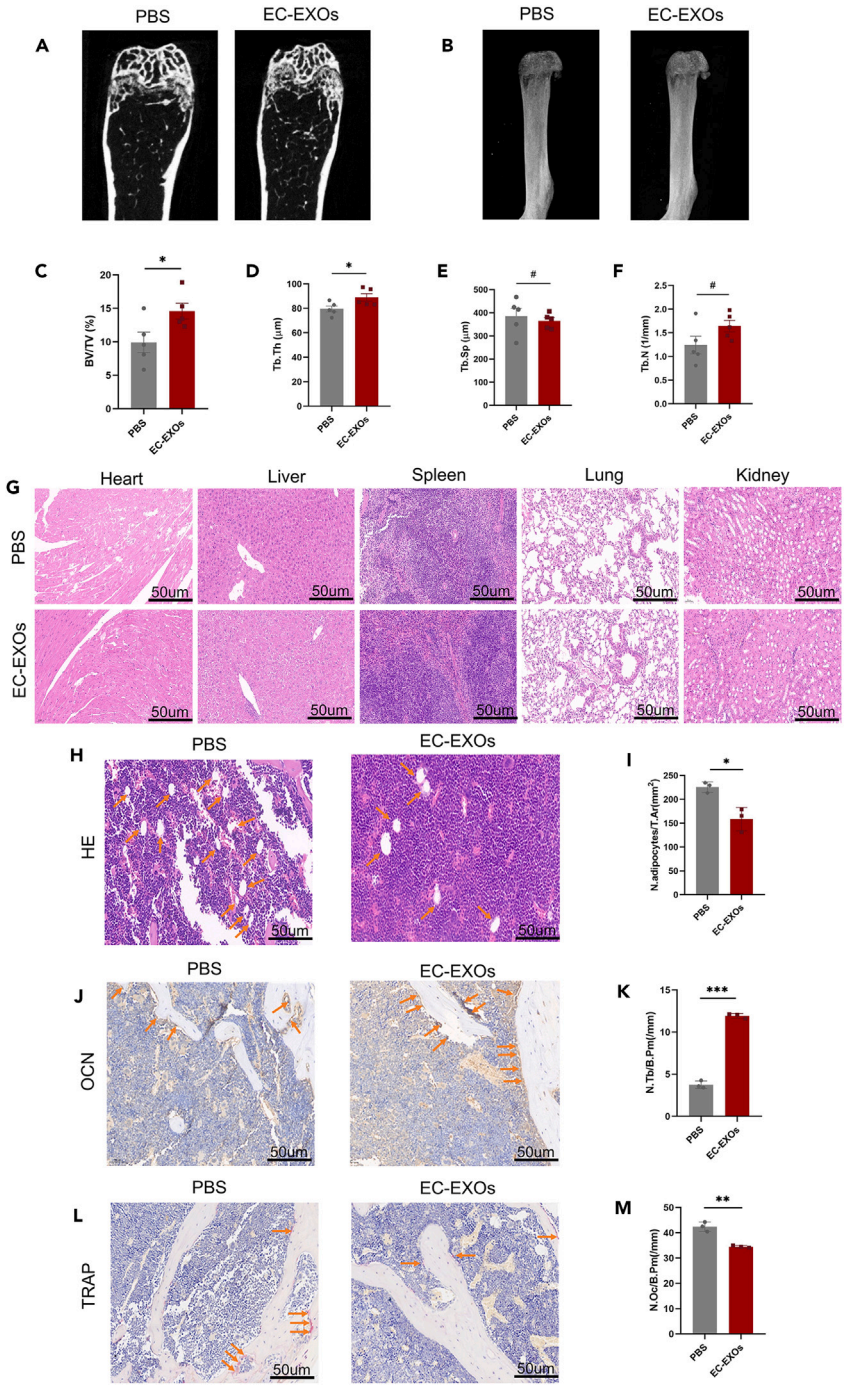

Figure 3. EC-EXOs increase bone formation and reduce bone marrow fat accumulation in aged mice

(A) Representative μCT images. Scale bar: 1 mm.

(B) 3D reconstruction figures of representative μCT.

(C–F) Quantitative analysis of the trabecular bone microarchitecture in the distal femurs of 15-month-old mice treated with PBS or EC-EXOs (BV/TV, Tb.N, Tb.Sp, and Tb.Th).

(G) Representative images of HE-stained heart, liver, spleen, lung, and kidney sections from 15-month-old mice treated with PBS or EC-EXOs. Scale bars: 50 μm.

(H) Representative images of HE staining of the distal femurs of 15-month-old mice treated with EC-EXOs or PBS and (I) quantification of the number of adipocytes associated with the tissue area (N.adipocytes/T.Ar) in the distal femur. Scale bar: 50 μm.

Figure 3. *Continued*

(J) Representative images of OCN staining and (K) quantification of osteoblast bone surface density (N.Ob/B.Pm) in the distal femurs of 15-month-old mice treated with PBS or EC-EXOs. Scale bar: 50 μm.

(L) Representative images of TRAP staining and (M) quantification of osteoclast bone surface density (N.Oc/B.Pm) in the distal femurs of 15-month-old mice treated with EC-EXOs or PBS. Scale bar: 50 μm. The values were expressed as mean ± SEM, *p < 0.05, **p < 0.01, ***p < 0.001.

cavity in the EC-EXO-treated mice than in the PBS-treated mice (Figures 3H and 3I). Immunohistochemical staining of OCN showed that EC-EXOs increased osteoblast cell formation in aged mice (Figures 3J and 3K). TRAP staining showed that fewer osteoclasts were deposited on the surface of cancellous bone in the experimental group than in the control group (Figures 3L and 3M). These results show that EC-EXOs promote bone formation, reduce fat formation, and inhibit osteoclast differentiation in aged mice.

EC-EXOs promote bone formation and reduce fat formation in OVX mice

To test the effect of EC-EXOs on ovariectomy (OVX) mice, we injected OVX mice with EC-EXOs (150 μg/100ul) three times a week via the tail vein. The ovaries of the OVX mice had obvious atrophy compared with those of the sham-operated mice (Figure 4A). Micro-CT analysis of 2D and 3D maps showed that bone mass was significantly greater in the EC-EXO-treated OVX mice than in the PBS-treated OVX mice (Figures 4B and 4C). Osteometric parameter analysis showed that the BV/TV, Tb.N, and Tb.Th values were greater, whereas the Tb.Sp value was lower, in the EC-EXO-treated OVX and sham groups of mice than in the PBS-treated OVX group of mice (Figures 4D–4G). HE staining showed that EC-EXOs had no effect on the physiological condition of the various organs of the OVX mouse model and resulted in no biocompatibility issues in OVX mice (Figure 4H). HE staining and quantification of femoral sections from OVX mice showed that EC-EXOs inhibited adipocyte formation in OVX mice (Figures 4I and 4J). EC-EXOs also promoted osteoblast deposition in OVX mice, as shown by OCN staining (Figures 4K–4L). Furthermore, TRAP staining showed that EC-EXOs inhibited osteoclast formation in OVX mice (Figures 4M–4N).

MiR-3p-975_4191 may be the critical factor in EC-EXOs mediating cell fate differentiation in BMSCs

Next, miRNA sequencing was used to screen the key factors regulating BMSC differentiation. miRNA sequencing analysis showed that 68 miRNAs were significantly upregulated, whereas 238 miRNAs were significantly downregulated, in HMEC-1-derived EC-EXOs compared with HMEC-1 cells (Figures 5A–5C). We also found that miR-3p-975_4191 had more notable changes in HMEC-1-derived EC-EXOs than in HMEC-1 cells (Figure 5D). RT-qPCR analysis showed that the miR-3p-975_4191 level was higher in EC-EXOs than in HMEC-1 cells, which was consistent with the sequencing results (Figure 5E). In addition, miR-3p-975_4191 upregulation was observed in BMSCs after treatment with EC-EXOs (Figure 5F). The previous results indicate that EC-EXOs may play a critical role in regulating the differentiation of BMSCs through miR-3p-975_4191.

Overexpression of miR-3p-975_4191 stimulates osteogenic differentiation of BMSCs

We further confirmed the regulatory effect of miR-3p-975_4191 on BMSC differentiation. After transfection with miR-3p-975_4191 mimic for 48 h, the level of miR-3p-975_4191 in BMSCs was approximately 40-fold higher than that in the negative control group, confirming the successful transfection of miR-3p-975_4191 mimic into BMSCs (Figure 6A). To elucidate the role of miR-3p-975_4191 in BMSC differentiation, we applied Alizarin red to measure the deposition of stromal calcium. As shown in the micrographs of Alizarin red staining, compared to the negative control, the miR-3p-975_4191 mimic greatly stimulated the osteogenic differentiation of BMSCs and increased calcium deposition (Figures 6B and 6C). In addition, miR-3p-975_4191 mimic treatment strongly increased the expression of osteogenesis-related genes, including ALP, POSTN, OC, COL1, BMP8a, and BSP, as shown by RT-qPCR analysis (Figures 6D–6I). We found that overexpression of miR-3p-975_4191 significantly promoted the osteogenic differentiation of BMSCs.

Overexpression of miR-3p-975_4191 inhibits adipogenic differentiation of BMSCs

To determine whether miR-3p-975_4191 has a regulatory role in the adipogenic differentiation of BMSCs, we transfected BMSCs with miR-3p-975_4191 mimic and stained them with Oil red O. Our results showed that overexpression of miR-3p-975_4191 decreased the formation of lipid droplets (Figures 6J and 6K). Furthermore, RT-qPCR analysis showed that overexpression of miR-3p-975_4191 significantly reduced the expression of the adipogenesis-related genes mPparg, CD36, and Cebpα (Figures 6L–6N). Together, these results confirm the inhibitory effect of miR-3p-975_4191 on BMSC adipogenic differentiation.

Knockdown of miR-3p-975_4191 inhibits BMSCs osteogenic differentiation

The regulatory effect of miR-3p-975_4191 on BMSC differentiation was verified by knocking down miR-3p-975_4191. After transfection with miR-3p-975_4191 inhibitor for 48 h, the level of miR-3p-975_4191 in BMSCs was about 10-fold lower than that of the negative control group, confirming that miR-3p-975_4191 inhibitor successfully transfected BMSCs (Figure 7A). Alizarin red-stained micrographs showed that miR-3p-975_4191 inhibitor greatly inhibited osteogenic differentiation of BMSCs and reduced calcium deposition compared with negative control (Figures 7B and 7C). In addition, RT-qPCR analysis showed that miR-3p-975_4191 inhibitor treatment strongly reduced the expression of osteogenesis-related genes, including RUNX2, BMP2, BSP, and COL1 (Figures 7D–7G). Thus, we found that knockdown of miR-3p-975_4191 significantly inhibited osteogenic differentiation of BMSCs.

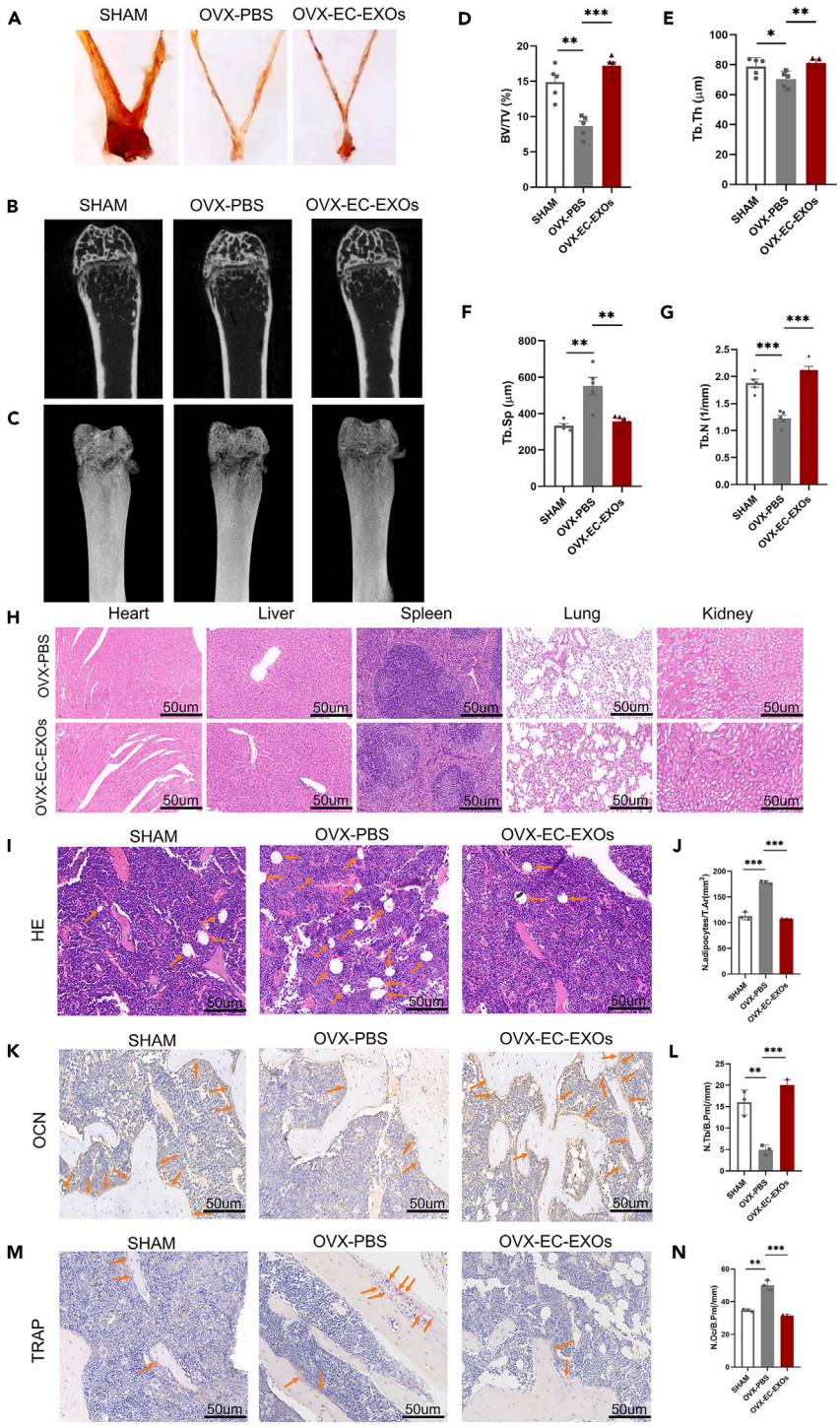

Figure 4. EC-EXOs promote bone formation and reduce fat formation in OVX mice

(A) Representative images of sham-operated mice and OVX mice.

(B) Representative μCT images. Scale bar: 1 mm.

(C) 3D reconstruction figures of representative μCT.

(D–G) Quantitative analysis of the trabecular bone microarchitecture in sham-operated mice and OVX mice treated with PBS or EC-EXOs (BV/TV, Tb.N, Tb.Sp, and Tb.Th).

(H) Representative images of HE-stained heart, liver, spleen, lung, and kidney sections from sham-operated mice and OVX mice treated with PBS or EC-EXOs. Scale bars: 50 μm.

Figure 4. *Continued*

(I) Representative images of HE staining of the distal femurs of sham-operated mice and OVX mice treated with PBS or EC-EXOs and (J) quantification of the number of adipocytes associated with the tissue area (N.adipocytes/T. Ar) in the distal femur. Scale bar: 50 μm.

(K) Representative images of OCN staining and (L) quantification of the osteoblast bone surface density (N.Ob/B.Pm) in the distal femurs of sham-operated mice and OVX mice treated with PBS or EC-EXOs. Scale bar: 50 μm.

(M) Representative images of TRAP staining and (N) quantification of osteoclast bone surface density (N.Oc/B.Pm) in the distal femurs of sham-operated mice and OVX mice treated with PBS or EC-EXOs. Scale bar: 50 μm. The values were expressed as mean ± SEM, *p < 0.05, **p < 0.01, ***p < 0.001.

Knockdown of miR-3p-975_4191 promotes lipidogenic differentiation of BMSCs

Knockdown of miR-3p-975_4191 further confirmed whether miR-3p-975_4191 has a regulatory role in lipidogenic differentiation of BMSCs. We transfected BMSCs with miR-3p-975_4191inhibitor and stained them with oil red O staining. The results showed that knockdown of miR-3p-975_4191 increased lipid droplet formation (Figures 7H and 7I). RT-qPCR analysis indicated that knockdown of miR-3p-975_4191 significantly enhanced the expression of adipogenesis-related genes mPparg, mFabp4, CD36, Hdipq, ID4, and LPL (Figures 7J–7O). Collectively, these results confirmed that knockdown of miR-3p-975_4191 promoted BMSC adipogenic differentiation.

MiR-3p-975_4191 regulates the differentiation of BMSCs through inhibition of TNF

To further confirm the mechanism by which miR-3p-975_4191 regulates the osteogenic differentiation and adipogenic differentiation of BMSCs, we conducted bioinformatics analysis. Venn diagram analysis identified 93 possible target genes shared by miR-3p-975_4191 and osteoporosis (Figure 8A). GO analysis (Figure 8B) of the selected miRNA target genes was performed to analyze the biological processes (Figure 8C), cellular components (Figure 8D), and molecular functions (Figure 8E) associated with the target genes. The target genes shared by miR-3p-975_4191 and osteoporosis was further analyzed by protein-protein interaction (PPI) network mapping, excluding nodes without protein interactions (Figure 8F). Visualization of the PPI network map was optimized by Cytoscape software (Figure 8G). The top 10 core target genes were then predicted based on the maximal clique centrality (MCC) algorithm (Figure 8H). By combining the previous bioinformatics results, we identified the core target gene TNF. TNF-α promotes osteoblast growth and DNA synthesis, inhibits alkaline phosphatase activity and contributes to impaired bone formation, so TNF may be a potential target of miR-3p-975_4191. Overexpression of miR-3p-975_4191 significantly downregulated TNF mRNA expression (Figure 8I). Western blot also confirmed that overexpression of miRNAs could downregulate TNF protein expression (Figure 8J). Knockdown of miR-3p-975_4191 during osteogenic induction and lipogenic induction of BMSCs, respectively, showed that both significantly upregulated TNF mRNA expression (Figure S2). To determine whether miR-3p-975_4191 directly binds to the 3′UTR of TNF and causes translational repression, we used dual-luciferase reporter assays in BMSCs. The miR-3p-975_4191 mimics significantly decreased the luciferase activity of the wild-type (WT) reporter, but did not affect the luciferase activity of the mutant reporter (Figures 8K and 8L). Taken together, these results suggest that miR-3p-975_4191 directly regulates the osteogenic-adipogenic fate differentiation of BMSCs by targeting TNF.

Curcumin inhibits adipogenic differentiation of BMSCs

To further explore treatment options for osteoporosis based on the therapeutic strategy of combining traditional Chinese medicine monomers with exosomes, we searched for traditional Chinese medicine monomers that can target TNF through the ETCM, Herb, and TCMSP databases. As shown in Table S1, 60 traditional Chinese medicine monomers were identified that can act on TNF. TNF is known to participate in the bone remodeling process through the MAPK, BMP/Smad, NF-κB, Wnt, Notch, and other signaling pathways.[11–14] Thus, our results suggested that the identified active ingredients of traditional Chinese medicines may affect the aforementioned signaling pathways by targeting TNF and thus treat osteoporosis. We next constructed a traditional Chinese medicine monomer—TNF signaling pathway—osteoporosis network with Cytoscape (Figure 9A). The detailed interactions between curcumin and TNF proteins were further investigated by molecular docking to predict their binding patterns and affinity in order to determine whether curcumin can influence the TNF pathway by binding to TNF proteins. The 2D interaction map (Figure 9B) of curcumin with TNF and the visualized 3D molecular docking map (Figure 9C) indicate that curcumin can stably bind to TNF. Our previous study confirmed that curcumin treats aging-related osteoporosis by promoting the osteogenic differentiation of BMSCs. Therefore, we selected curcumin, an active component of a Chinese medicine, for subsequent investigation of its ability to act in concert with EC-EXOs to achieve osteogenic and adipogenic differentiation of BMSCs. The CCK-8 results showed that curcumin below 5 μM was less toxic to BMSCs than the control (Figure 9D). To further study the effect of curcumin on the adipogenic differentiation of BMSCs, we treated BMSCs with PBS, 1 μM curcumin, 2 μM curcumin, and 5 μM curcumin and investigated the formation of lipid droplets. BMSCs in different groups were cultured in adipogenic induction medium for 14 days, stained with Oil red O, and examined. The results showed that compared to PBS, curcumin dose-dependently decreased lipid droplet formation in the BMSCs (Figures 9E and 9F). In addition, RT-qPCR showed that curcumin significantly reduced the expression of mFabp4, mPparg, Cebp-α, and GPD1, which are related to adipogenic differentiation (Figures 9G–9J). Thus, the results show that curcumin can significantly inhibit the adipogenic differentiation of BMSCs.

Curcumin combined with EC-EXOs synergistically promotes the osteogenic differentiation of BMSCs

To further investigate whether curcumin has a synergistic effect on the differentiation of BMSCs by binding with EC-EXOs, we treated BMSCs with curcumin and EC-EXOs (25 μg/mL) for 21 days in osteogenic induction medium. Alizarin red staining and quantitative analysis showed

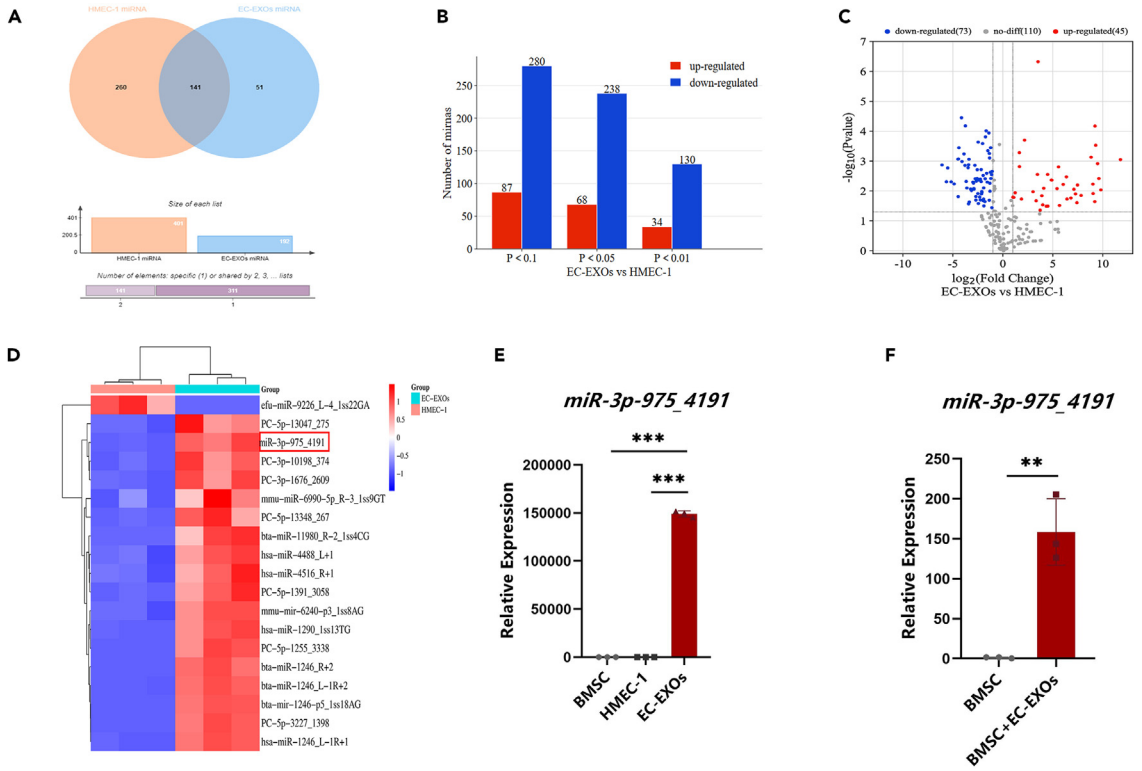

Figure 5. Identification of differentially expressed miRNAs between HMEC-1 cells and EC-EXOs

(A) Venn diagram showing the overlap of shared miRNAs in HMEC-1 cells and EC-EXOs.

(B) Histogram showing the number of differentially expressed miRNAs between HMEC-1 cells and EC-EXOs. Blue and red indicate downregulation and upregulation, respectively.

(C) Volcano plot of sequencing analysis of miRNAs differentially expressed between HMEC-1 cells and EC-EXOs. Blue and red indicate downregulation and upregulation, respectively.

(D) Heatmap of cluster analysis of differential expression of miRNAs between HMEC-1 cells and EC-EXOs. miRNA expression is presented as the log10(norm value). Red indicates strongly expressed genes, and blue indicates weakly expressed genes.

(E) Expression of miR-3p-975_4191 in BMSCs, HMEC-1 cells and EC-EXOs as verified by RT-qPCR.

(F) Expression of miR-3p-975_4191 in BMSCs and BMSCs treated with EC-EXOs as verified by RT-qPCR. The values were expressed as mean ± SEM, *p < 0.05, **p < 0.01, ***p < 0.001.

that curcumin coactivated the osteogenic differentiation of BMSCs with EC-EXOs (Figures 10A and 10B). RT-qPCR experiments further confirmed that the expression of osteogenesis-related genes, including ALP, OPN, and OC, was activated to a greater extent in the cotreatment group than in the groups treated with either curcumin or EC-EXOs alone (Figures 10C–10E). Taken together, these results suggest that curcumin and EC-EXOs can act synergistically to promote the osteogenic differentiation of BMSCs.

Curcumin combined with EC-EXOs exerts a synergistic effect to inhibit the adipogenic differentiation of BMSCs

Next, we investigated the synergistic effect of curcumin and EC-EXOs on the adipogenic differentiation of BMSCs. BMSCs were treated with curcumin and EC-EXOs (25 μg/mL) for 21 days in adipogenic induction medium. The results of Oil red O staining and quantification showed that curcumin combined with EC-EXO treatment inhibited adipogenic differentiation of BMSCs more effectively than curcumin or EC-EXO treatment alone, with a significant reduction in lipid droplet formation (Figures 10F and 10G). This finding was also confirmed by RT-qPCR experiments, in which the expression levels of the lipid-related genes mFabp4, mPparg, and Cebpα were all lower in the combined treatment group than in the individual treatment groups (Figures 10H–10J). In summary, these results suggest that curcumin and EC-EXOs can act synergistically to inhibit the adipogenic differentiation of BMSCs.

DISCUSSION

Osteoporosis is a common systemic bone disease that causes bone fragility and an increased risk of fracture.[15] Further studies on the bone marrow microenvironment are essential for the development of strategies to slow the progression of osteoporosis. In this study, EC-EXOs were found to promote the osteogenic differentiation of BMSCs and inhibit the adipogenic differentiation of BMSCs. Through differential

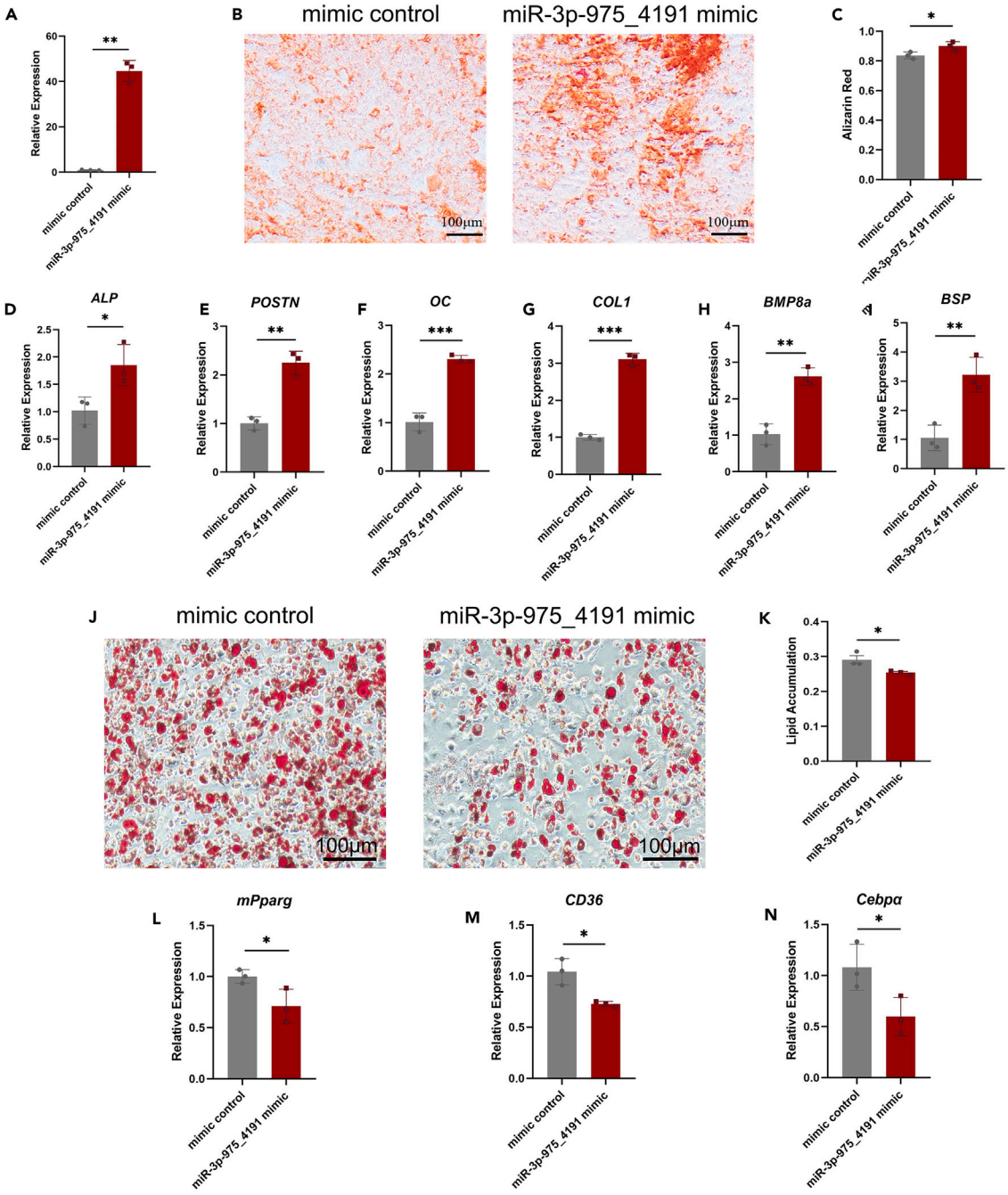

Figure 6. Overexpression of miR-3p-975_4191 can promote osteogenic differentiation and inhibit adipogenic differentiation of BMSCs

(A) The overexpression of miR-3p-975_4191 in BMSCs after gene transfection was verified by RT-qPCR. Representative images of Alizarin red staining after 21 days of osteogenic induction (B) and quantification of calcification (C) of BMSCs after overexpression of miR-3p-975_4191. Scale bar, 100 μm.

(D–I) The mRNA expression levels of osteogenic biomarkers (ALP, POSTN, OC, COL1, BMP8a and BSP) in osteogenically differentiated BMSCs after overexpression of miR-3p-975_4191 on Day 7 were detected by RT-qPCR. Oil red O staining (J) and quantification (K) of BMSCs after 14 days of adipogenic induction after overexpression of miR-3p-975_4191. Scale bar, 100 μm.

(L–N) The mRNA expression levels of adipogenic biomarkers (mPparg, CD36, and Cebpα) in adipogenically differentiated BMSCs in different groups after overexpression of miR-3p-975_4191 on Day 7 were detected by RT-qPCR. β-Actin was used as an internal control. The values were expressed as mean ± SEM, *$p < 0.05$, **$p < 0.01$, ***$p < 0.001$.

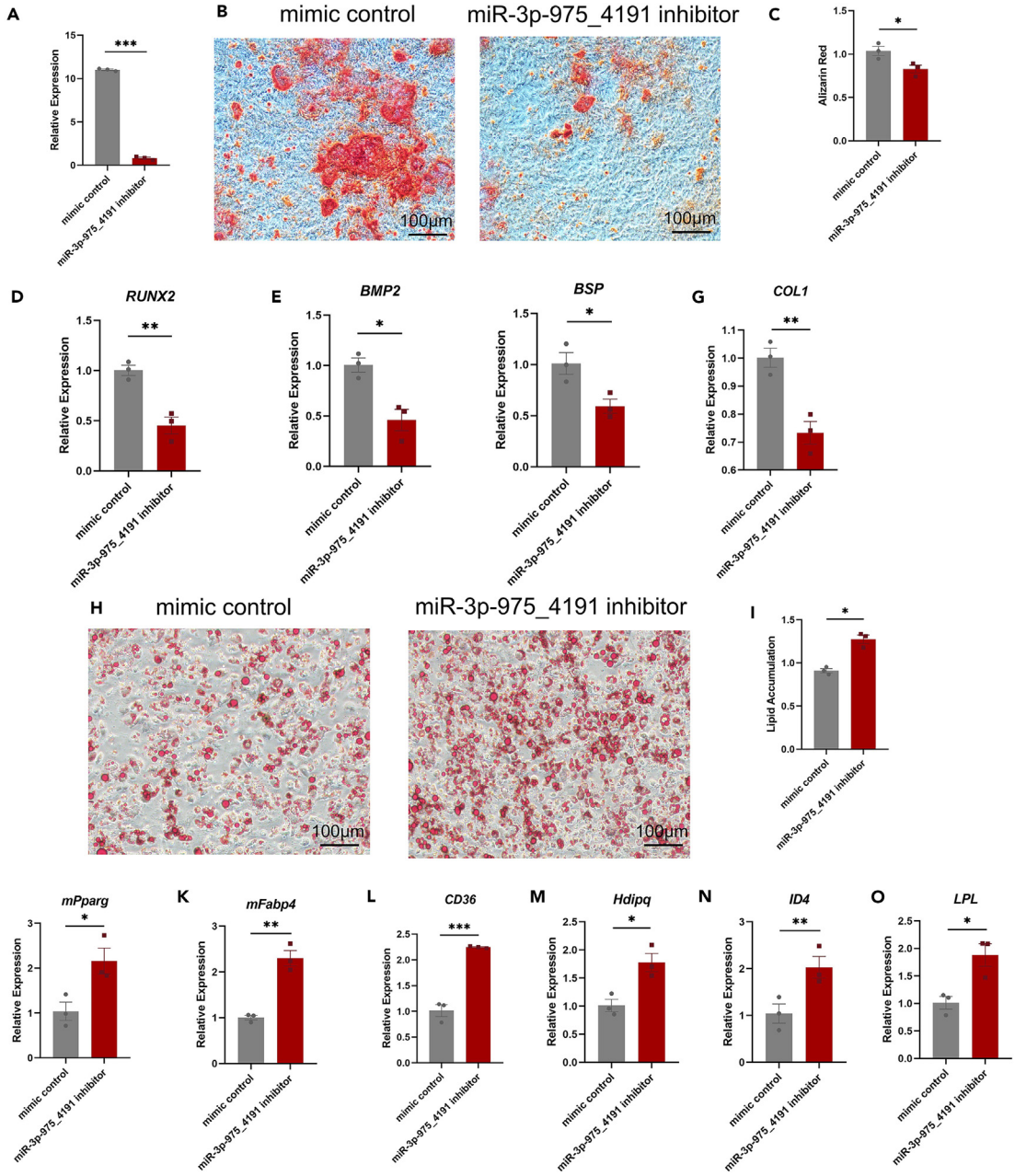

Figure 7. Knockdown of miR-3p-975_4191 can inhibit osteogenic differentiation and promote adipogenic differentiation of BMSCs

(A) Knockdown of miR-3p-975_4191 in BMSCs after gene transfection was verified by RT-qPCR. Representative images of Alizarin red staining after 21 days of osteogenic induction (B) and quantification of calcification (C) of BMSCs after knockdown of miR-3p-975_4191. Scale bar, 100 μm.

(D–G) The mRNA expression levels of osteogenic biomarkers (RUNX2, BMP2, BSP, and COL1) in osteogenically differentiated BMSCs after knockdown of miR-3p-975_4191 on Day 7 were detected by RT-qPCR. Oil red O staining (H) and quantification (I) of BMSCs after 14 days of adipogenic induction after knockdown of miR-3p-975_4191. Scale bar, 100 μm.

(J–O) The mRNA expression levels of adipogenic biomarkers (mPparg, mFabp4, CD36, Hdipq, ID4, and LPL) in adipogenically differentiated BMSCs in different groups after knockdown of miR-3p-975_4191 on Day 7 were detected by RT-qPCR. β-Actin was used as an internal control. The values were expressed as mean ± SEM, *$p < 0.05$, **$p < 0.01$, ***$p < 0.001$.

miRNA clustering analysis, we identified miR-3p-975_4191 as a miRNA with higher expression in EC-EXOs than in HMEC-1 cells. MiR-3p-975_4191 downregulated TNF expression, inhibited osteoblast differentiation and promoted adipogenic differentiation of BMSCs. Based on the network pharmacology screen and our previous findings, we further investigated whether curcumin also targeted TNF and played

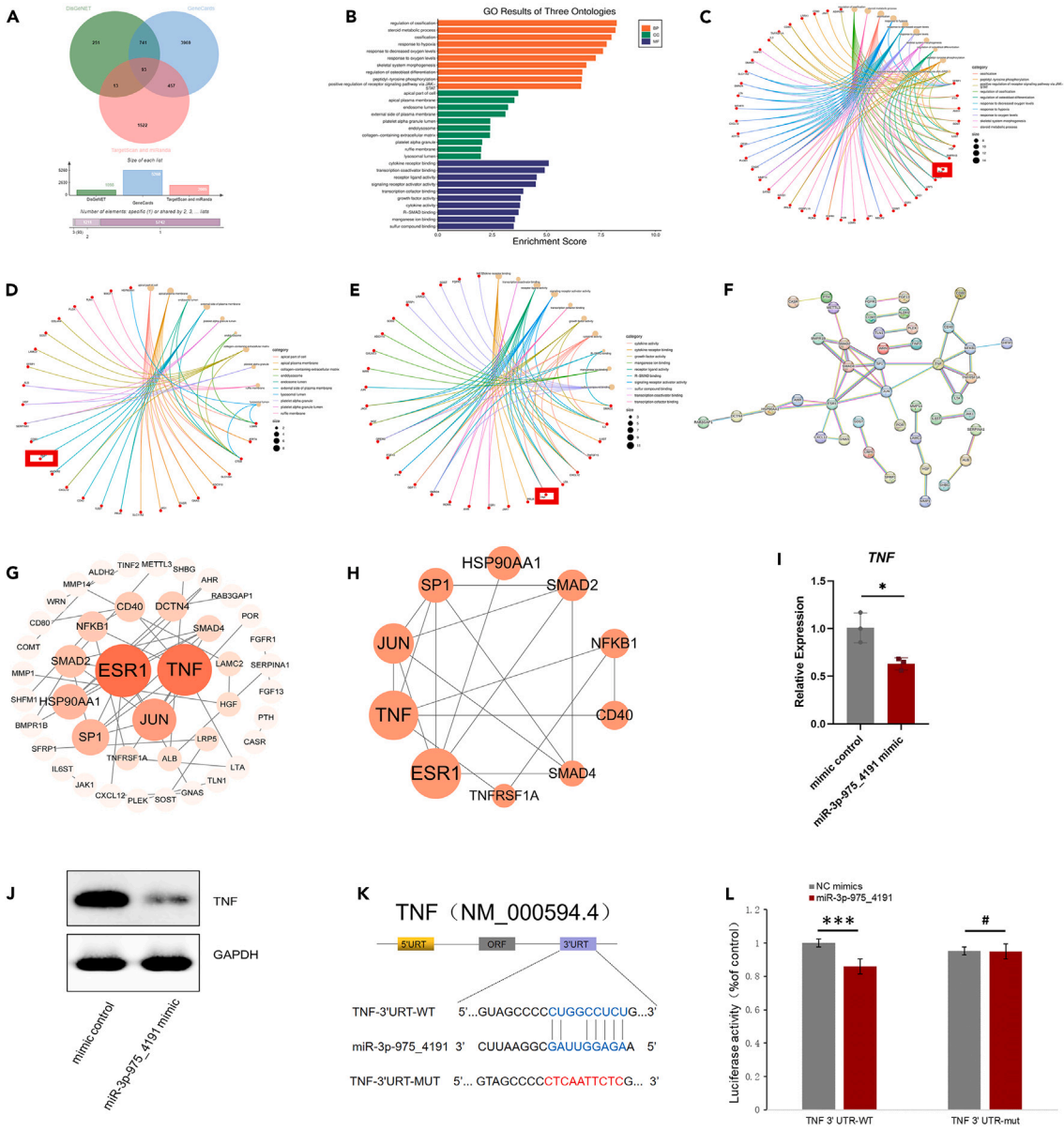

Figure 8. TNF is a potential target gene for miR-3p-975_4191

(A) Venn diagram showing the shared target genes of miR-3p-975_4191 and osteoporosis.

(B) The corresponding GO annotations of the selected miRNA target genes were determined, and the GO functions of each class were ranked from highest to lowest according to the number of annotated target genes. The horizontal coordinate is the enrichment score, and the vertical coordinate is the GO classification. The circle diagram shows the biological process (C), cell component (D) and molecular function (E) terms associated with the miR-3p-975_4191 target genes.

(F) PPI network map of the shared target genes of miR-3p-975_4191 and osteoporosis, excluding nodes without protein interactions. The confidence level was 0.9.

(G) PPI network diagram optimized by Cytoscape software.

(H) Hub network diagram of the top 10 core target genes based on the MCC algorithm.

(I) The expression of TNF after overexpression of miR-3p-975_4191 was verified by RT-qPCR.

(J) The expression of TNF protein was detected by western blot after overexpression of miR-3p-975_4191.

(K) The potential binding sites for miR-3p-975_4191 on the 3′UTR of TNF.

(L) BMSCs were transfected with a luciferase reporter vector containing either the WT or mutant plasmid of the 3′UTR of TNF. The values were expressed as mean ± SEM, *p < 0.05, **p < 0.01, ***p < 0.001.

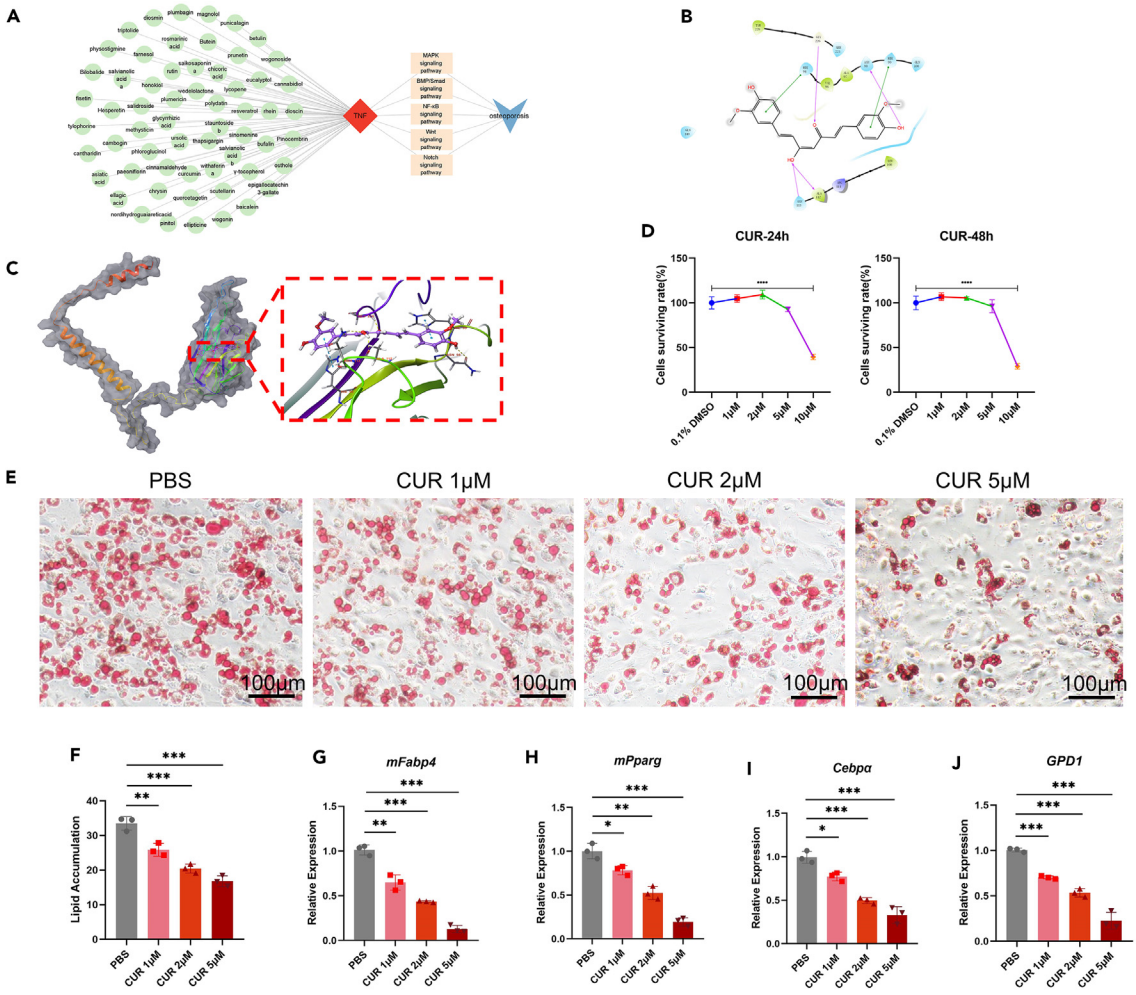

Figure 9. Curcumin can inhibit adipogenic differentiation of BMSCs

(A) Construction of a Chinese medicine monomer active ingredient-TNF signaling pathway-osteoporosis network using Cytoscape.

(B) Two-dimensional diagram of the interaction of curcumin with TNF.

(C) Visualization of the molecular docking of curcumin with TNF in 3D.

(D) CCK-8 assay to analyze the cytotoxicity of curcumin.

(E) Oil red O staining and (F) quantification of BMSCs after adipogenic induction for 14 days among different groups. Scale bar, 100 μm.

(G–J) The mRNA expression levels of adipogenic biomarkers (mFabp4, mPparg, Cebpα, and GPD1) in adipogenically differentiated BMSCs in different groups on Day 7 were detected by RT-qPCR. β-Actin was used as an internal control. The values were expressed as mean ± SEM, *$p < 0.05$, **$p < 0.01$, ***$p < 0.001$.

a positive role in BMSC fate differentiation. EC-EXOs combined with curcumin even more effectively promoted osteogenic differentiation and inhibited adipogenic differentiation of BMSCs. Taken together, our results demonstrate that EC-EXOs may exert a synergistic effect with curcumin to regulate the fate differentiation of BMSCs through miR-3p-975_4191-mediated targeting of TNF and may play an essential role in slowing the process of osteoporosis, providing different ideas for better clinical treatment of osteoporosis.

In recent years, an increasing number of studies have reported on the osteogenic effects of exosomes. Exosome-based delivery of bone-targeted drugs can alleviate impaired bone formation and bone loss.[16] Liu et al. revealed that bone marrow stromal cell-derived exosomes significantly promote osteogenic differentiation of BMSCs *in vitro*, and BMSC-specific aptamer-functionalized bone marrow stromal cell-derived exosomes that target bone are highly effective in promoting bone regeneration.[17] Previous studies have suggested that BMSC-derived exosomes can promote osteogenesis and angiogenesis.[18] In addition, research by Song et al. has confirmed that EC-EXOs show more effective bone targeting than osteoblast-derived or BMSC-derived exosomes and can inhibit osteoclast activity *in vitro*.[19] In our study, we observed dose-dependent increases in mineral deposition in BMSCs treated with different concentrations of EC-EXOs. The expression of the osteogenic genes RUNX2 and OPN was also increased in BMSCs after EC-EXO treatment. This finding was consistent with the results of previous studies on the osteogenic role of exosomes. In contrast, our group identified the important role of EC-EXOs in promoting the osteogenic differentiation of BMSCs. Furthermore, we found a dose-dependent reduction in lipid droplet formation and a decrease in

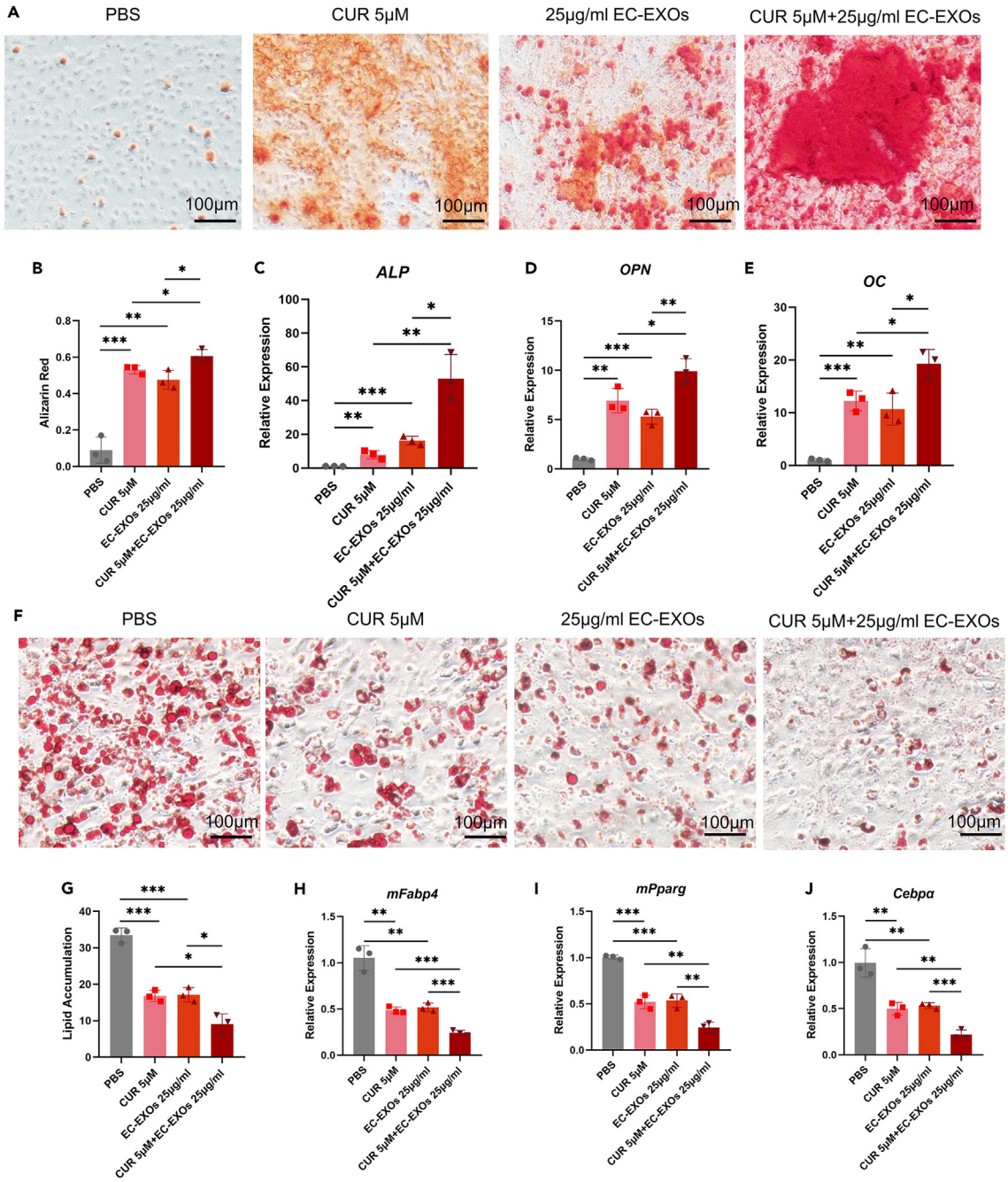

Figure 10. Curcumin combined with EC-EXOs synergistically promotes osteogenic differentiation and inhibits adipogenic differentiation of BMSCs

(A) Representative images of Alizarin red staining after 21 days of osteogenic induction and (B) quantification of calcification of BMSCs among different groups. Scale bar, 100 μm.

(C–E) mRNA expression levels of osteogenic biomarkers (ALP, OPN, and OC) in osteogenically differentiated BMSCs in different groups on Day 7 were detected by RT-qPCR.

(F) Oil red O staining and (G) quantification of BMSCs after adipogenic induction for 14 days among different groups. Scale bar, 100 μm.

(H–J) The mRNA expression levels of adipogenic biomarkers (mFabp4, mPparg, and Cebpα) in adipogenically differentiated BMSCs in different groups on Day 7 were detected by RT-qPCR. β-Actin was used as an internal control. The values were expressed as mean ± SEM, *p < 0.05, **p < 0.01, ***p < 0.001.

lipogenesis-related gene expression in BMSCs treated with different concentrations of EC-EXOs, confirming that EC-EXOs affect the adipogenic differentiation and the osteogenic differentiation of BMSCs in opposite directions. In summary, we confirmed the role of EC-EXOs in regulating the fate differentiation of BMSCs *in vitro*. We also constructed an OVX model and a senescent mouse model to further investigate

the effects of EC-EXOs *in vivo*. Micro-CT analysis and OCN staining showed that EC-EXOs increased cancellous bone formation and increased the number of osteoblasts in aged mice and in OVX model mice. Correspondingly, HE and TRAP staining confirmed that EC-EXO treatment reduced the numbers of adipocytes and osteoclasts. Xin et al. showed that exosomes secreted by human induced pluripotent stem cell-derived mesenchymal stem cells (MSC) were effective in promoting osteogenic differentiation in an OVX mouse model and that the effect increased with increasing exosome concentrations.[20] Wang et al. showed that adipocyte-derived exosomes not only improved bone microarchitecture but also significantly reduced bone marrow fat accumulation.[21] There were similarities between our study and theirs, but ours demonstrated the role of EC-EXOs in promoting osteogenesis and inhibiting lipogenesis. Our study substantiated through *in vitro* and *in vivo* experiments that EC-EXOs play an instrumental role in slowing the process of osteoporosis.

MiRNAs that influence translation and mRNA stability have emerged as important regulators of gene expression.[22–24] These molecules can induce a variety of changes in cellular processes including cell proliferation, cell differentiation, and cellular senescence.[23,25] Zhu et al. found that miRNAs contained in exosomes can enhance osteoblast differentiation through paracrine and proximal secretory mechanisms and have a central coupling function in bone formation.[26] MiRNAs may be intertwined with vascular secretory factors released from vascular-specific ECs to exhibit key functions in the angiogenesis-osteogenesis coupling that is essential to bone remodeling.[26] For example, the role of BMSC-derived exosomal miR-29a in promoting angiogenesis and osteogenesis has been demonstrated both *in vitro* and *in vivo*. BMSCs-Exos loaded with miR-29a may be a potential therapeutic target for osteoporosis.[18] In addition, Yang's study elucidated the potential functional relevance of MALAT1-containing exosomes derived from BMSC in osteoporosis. By mediating miR-34c/SATB2 binding, BMSC-derived exosomal MALAT1 enhances osteoblast activity in osteoporotic mice.[27] The study by Cui et al. developed a special exosome delivery system that is based on exosomes secreted from MSC of human induced pluripotent stem cells (iPSC). These engineered exosomes, BT-Exo-si Shn3, utilize the intrinsic anti-osteoporotic function of these particular MSC-derived exosomes and synergize with the loaded siRNA of the Shn3 gene to enhance the therapeutic effect.[28] Another study showed that nanovesicles targeting bone marrow endothelial cells (BMECs) treat osteoporosis by altering the endothelium-associated secretory phenotype of bone. It was shown that due to the unique endogenous miRNA cargo of bioinspired nanovesicles (BNVs), these BNVs re-educate BMECs to secrete cytokines that favor osteogenesis and anti-inflammation. As a result of the secreted phenotypic transformation, osteogenic differentiation of bone MSC was promoted and the pro-inflammatory microenvironment in osteoporotic bone, dominated by M1 macrophages, was improved.[29] Li et al. showed that the dual regulatory strategy of physical barrier to bone matrix and intracellular gene regulation generated by advanced biomaterials is a viable option for the treatment of postmenopausal osteoporosis (PMOP). They designed an osteophilic and dual-regulated alendronate-gene lipoplex (antagomir@Aln-Lipo) consisting of alendronate-functionalized liposomal carriers and encapsulated specific microRNAs for bone-targeted delivery of genes to achieve combined relief of bone loss. These functionalized lipid complexes exhibit long-term stability and excellent transfection efficiency. The osteophilic and dually regulated isotype replacement antibody @ Aln-Lipo provides a bifunctional strategy for precision therapy of PMOP.[30] Through miRNA-seq sequencing, we screened for key factors by which EC-EXOs regulate the fate differentiation of BMSCs. Our study showed that the expression of miR-3p-975_4191 was significantly greater in EC-EXOs than in BMSCs and HMEC-1 cells. Overexpression of miR-3p-975_4191 greatly stimulated osteoblast differentiation in BMSCs, and Alizarin red staining showed increased calcium deposition. Moreover, overexpression of miR-3p-975_4191 substantially increased the expression levels of ALP, POSTN, OC, COL1, BMP8a and BSP, which are markers of osteogenic differentiation. Jih-Yang Ko's study suggested that reduced miRNA expression levels are associated with fat accumulation in the bone marrow.[31] Our study further supports this result and reveals that miR-3p-975_4191 overexpression can inhibit the adipogenic differentiation of BMSCs, suppressing the formation of lipid droplets in BMSCs. Knockdown of miR-3p-975_4191 yielded the exact opposite conclusion, and also laterally confirmed the important role of miR-3p-975_4191 in BMSCs fate differentiation. To confirm the mechanism of the effect of miR-3p-975_4191 on the fate differentiation of BMSCs, we performed bioinformatics analysis and screened TNF as the core target gene. Overexpression of miR-3p-975_4191 derived from EC-EXOs led to decreased TNF expression in BMSCs. Previous studies have shown that TNF is a key cytokine regulator of bone that mediates inflammatory bone loss.[32] Inactivation of TNF-α has been found to reduce bone loss in a mouse model.[33] Furthermore, clinical trials by Wijbrandts et al. have demonstrated that TNF blockade may lead to a cessation of bone loss.[34] Our study confirms the role of TNF.

An in-depth screening of traditional Chinese medicine monomers acting on TNF revealed that curcumin can also target TNF. Our previous study confirmed that curcumin promoted the osteogenic differentiation of BMSCs. In the present study, we demonstrated that curcumin inhibited the adipogenic differentiation of BMSCs. Curcumin has a unique structure, significant activity, high efficacy, and few side effects.[35] Research on the use of curcumin for osteoporosis prevention or treatment has been conducted nationally and internationally.[36–38] For example, Heo's study showed that cyclodextrin/curcumin complexes significantly improved bone density and prevented bone loss in an OVX mouse model.[39] Chen et al. indicated that curcumin may be a promising agent for the prevention and treatment of glucocorticoid-induced osteoporosis.[40] The findings of our study were consistent with those of these previous studies. The combination of exosomes and drugs may be a valid strategy for treating disease. Studies have shown that the combination of neuronal cell-derived exosomes and levodopa could be an effective potential treatment for Parkinson's disease.[41] Mohsen et al. found that exosomes derived from BMSCs in combination with Rosuvastatin were beneficial for functional recovery in ischemic stroke rats.[42] Imatinib combined with exosomes from mesenchymal stromal cells significantly improved the outcome of chronic granulocytic leukemia.[43] However, the combination of exosomes and drugs for the treatment of osteoporosis has not yet been reported. Based on previous research we treated BMSCs with curcumin in combination with EC-EXOs and found that the combination had a better bone-enhancing effect than either treatment alone. This proves that curcumin can target TNF and may act synergistically with EC-EXOs to regulate the differentiation of BMSCs. Furthermore, our study

demonstrates that the combination of curcumin with EC-EXOs may have crucial implications for improved clinical management of osteoporosis. Our findings suggest that EC-EXOs may exert a synergistic effect with curcumin in reversing the progression of osteoporosis by targeting TNF via miR-3p-975_4191. This may provide clinical ideas for more effective prevention and treatment of osteoporosis.

Limitations of the study

In this study, the effect of EC-EXOs on the fate differentiation of BMSCs was verified at the cellular and animal levels, but only at the cellular level, the effect of EC-EXOs in combination with curcumin on the fate differentiation of BMSCs by acting on TNF targets was verified, and the subsequent experiments need to be further supplemented with animal experiments on the combined effect. In addition, this study has not been further explored for its possible clinical application, which needs to be further supplemented in subsequent experiments.

STAR★METHODS

Detailed methods are provided in the online version of this paper and include the following:

- KEY RESOURCES TABLE
- RESOURCE AVAILABILITY
  - Lead contact
  - Materials availability
  - Data and code availability
- EXPERIMENTAL MODEL AND STUDY PARTICIPANT DETAILS
  - Statement of ethics
  - Animal models
- METHOD DETAILS
  - Isolation of mouse BMSCs
  - Isolation and characterization of exosomes
  - Transmission electron microscopy (TEM)
  - Nanoparticle tracking analysis (NTA)
  - Exosome labeling and coculture with BMSCs
  - Western blot analysis
  - Adipogenic differentiation
  - Osteogenic differentiation
  - Oil red O staining and quantitative analysis
  - Alizarin red staining and quantitative analysis
  - Quantitative real-time PCR (qRT–PCR) analysis
  - Animal model and grouping
  - Micro-CT analysis
  - Histochemistry and immunocytochemistry
  - Microarray analysis
  - Cell transfection
  - Cell counting kit-8 (CCK-8) assay
- QUANTIFICATION AND STATISTICAL ANALYSIS

SUPPLEMENTAL INFORMATION

Supplemental information can be found online at https://doi.org/10.1016/j.isci.2024.109608.

ACKNOWLEDGMENTS

Graphical abstract was created with BioRender.com. The authors thank Springer Nature Author Services (https://authorservices.springernature.com/) for the English language editing and review services. This work was supported by the China National Key R&D Program (Nos2020YFC2009000 and 2020YFC2009001), the Hunan Provincial Department of Finance Gra (2022-151, 2021-139, 2020-83, 2019-93, and 2018-92), Hunan Provincia Development and Reform Commission of Innovastive Research Program (2021-212-23), Hunan Innovative Province Construction Special Project (2021ZK4025), and Natural Science Foundation of Hunan Province (2020JJ4799).

AUTHOR CONTRIBUTIONS

W.J.J. conceptualization, participation in experiments, data curation, writing-original draft preparation; X.X.Y. methodology, participation in selected experiments, data curation; L.H. participation in selected experiments, data curation; Z.Q.Y. data curation; C.Y. methodology; C.W.J. contributed to the discussion; C.Y.J. conceptualization; H.J.Y. contributed to the discussion; L.Q. writing-review and editing. All the authors have accepted responsibility for the entire content of this submitted manuscript and approved submission.

DECLARATION OF INTERESTS

The authors declare no competing interests.

Received: August 28, 2023
Revised: February 22, 2024
Accepted: March 25, 2024
Published: March 27, 2024

REFERENCES

1. Fang, Y., Zhu, J., Fan, J., Sun, L., Cai, S., Fan, C., Zhong, Y., and Li, Y. (2021). Dietary Inflammatory Index in relation to bone mineral density, osteoporosis risk and fracture risk: a systematic review and meta-analysis. Osteoporos. Int. *32*, 633–643. https://doi.org/10.1007/s00198-020-05578-8.
2. Cauley, J.A. (2017). Osteoporosis: fracture epidemiology update 2016. Curr. Opin. Rheumatol. *29*, 150–156. https://doi.org/10.1097/bor.0000000000000365.
3. Peng, Y., Wu, S., Li, Y., and Crane, J.L. (2020). Type H blood vessels in bone modeling and remodeling. Theranostics *10*, 426–436. https://doi.org/10.7150/thno.34126.
4. Biswas, L., Chen, J., De Angelis, J., Singh, A., Owen-Woods, C., Ding, Z., Pujol, J.M., Kumar, N., Zeng, F., Ramasamy, S.K., and Kusumbe, A.P. (2023). Lymphatic vessels in bone support regeneration after injury. Cell *186*, 382–397.e324. https://doi.org/10.1016/j.cell.2022.12.031.
5. Maes, C., Kobayashi, T., Selig, M.K., Torrekens, S., Roth, S.I., Mackem, S., Carmeliet, G., and Kronenberg, H.M. (2010). Osteoblast precursors, but not mature osteoblasts, move into developing and fractured bones along with invading blood vessels. Dev. Cell *19*, 329–344. https://doi.org/10.1016/j.devcel.2010.07.010.
6. Yu, M., Liu, W., Li, J., Lu, J., Lu, H., Jia, W., and Liu, F. (2020). Exosomes derived from atorvastatin-pretreated MSC accelerate diabetic wound repair by enhancing angiogenesis via AKT/eNOS pathway. Stem Cell Res. Ther. *11*, 350. https://doi.org/10.1186/s13287-020-01824-2.
7. Elsharkasy, O.M., Nordin, J.Z., Hagey, D.W., de Jong, O.G., Schiffelers, R.M., Andaloussi, S.E., and Vader, P. (2020). Extracellular vesicles as drug delivery systems: Why and how? Adv. Drug Deliv. Rev. *159*, 332–343. https://doi.org/10.1016/j.addr.2020.04.004.
8. Alvarez-Erviti, L., Seow, Y., Yin, H., Betts, C., Lakhal, S., and Wood, M.J. (2011). Delivery of siRNA to the mouse brain by systemic injection of targeted exosomes. Nat. Biotechnol. *29*, 341–345. https://doi.org/10.1038/nbt.1807.
9. Li, S., Stöckl, S., Lukas, C., Herrmann, M., Brochhausen, C., König, M.A., Johnstone, B., and Grässel, S. (2021). Curcumin-primed human BMSC-derived extracellular vesicles reverse IL-1β-induced catabolic responses of OA chondrocytes by upregulating miR-126-3p. Stem Cell Res. Ther. *12*, 252. https://doi.org/10.1186/s13287-021-02317-6.
10. Wu, W., Xia, C., Xie, X., Li, H., Wang, J., Liu, T., et al. (2021). Effect of curcumin on bone metabolic homeostasis in mice with aging-associated osteoporosis. Central South Pharmacy *19*, 1108–1113.
11. Feng, G., Zheng, K., Song, D., Xu, K., Huang, D., Zhang, Y., Cao, P., Shen, S., Zhang, J., Feng, X., and Zhang, D. (2016). SIRT1 was involved in TNF-α-promoted osteogenic differentiation of human DPSCs through Wnt/β-catenin signal. In Vitro Cell. Dev. Biol. Anim. *52*, 1001–1011. https://doi.org/10.1007/s11626-016-0070-9.
12. Zhao, B. (2017). TNF and Bone Remodeling. Curr. Osteoporos. Rep. *15*, 126–134. https://doi.org/10.1007/s11914-017-0358-z.
13. Xia, Y., Inoue, K., Du, Y., Baker, S.J., Reddy, E.P., Greenblatt, M.B., and Zhao, B. (2022). TGFβ reprograms TNF stimulation of macrophages towards a non-canonical pathway driving inflammatory osteoclastogenesis. Nat. Commun. *13*, 3920. https://doi.org/10.1038/s41467-022-31475-1.
14. Kang, X., Chen, L., Yang, S., Gong, Z., Hu, H., Zhang, X., Liang, C., and Xu, Y. (2022). Zuogui Wan slowed senescence of bone marrow mesenchymal stem cells by suppressing Wnt/β-catenin signaling. J. Ethnopharmacol. *294*, 115323. https://doi.org/10.1016/j.jep.2022.115323.
15. Ensrud, K.E., and Crandall, C.J. (2017). Osteoporosis. Ann. Intern. Med. *167*. Itc17-itc32. https://doi.org/10.7326/aitc201708010.
16. Guo, J., Wang, F., Hu, Y., Luo, Y., Wei, Y., Xu, K., Zhang, H., Liu, H., Bo, L., Lv, S., et al. (2023). Exosome-based bone-targeting drug delivery alleviates impaired osteoblastic bone formation and bone loss in inflammatory bowel diseases. Cell Rep Med *4*, 100881. https://doi.org/10.1016/j.xcrm.2022.100881.
17. Luo, Z.W., Li, F.X., Liu, Y.W., Rao, S.S., Yin, H., Huang, J., Chen, C.Y., Hu, Y., Zhang, Y., Tan, Y.J., et al. (2019). Aptamer-functionalized exosomes from bone marrow stromal cells target bone to promote bone regeneration. Nanoscale *11*, 20884–20892. https://doi.org/10.1039/c9nr02791b.
18. Lu, G.D., Cheng, P., Liu, T., and Wang, Z. (2020). BMSC-Derived Exosomal miR-29a Promotes Angiogenesis and Osteogenesis. Front. Cell Dev. Biol. *8*, 608521. https://doi.org/10.3389/fcell.2020.608521.
19. Song, H., Li, X., Zhao, Z., Qian, J., Wang, Y., Cui, J., Weng, W., Cao, L., Chen, X., Hu, Y., and Su, J. (2019). Reversal of Osteoporotic Activity by Endothelial Cell-Secreted Bone Targeting and Biocompatible Exosomes. Nano Lett. *19*, 3040–3048. https://doi.org/10.1021/acs.nanolett.9b00287.
20. Qi, X., Zhang, J., Yuan, H., Xu, Z., Li, Q., Niu, X., Hu, B., Wang, Y., and Li, X. (2016). Exosomes Secreted by Human-Induced Pluripotent Stem Cell-Derived Mesenchymal Stem Cells Repair Critical-Sized Bone Defects through Enhanced Angiogenesis and Osteogenesis in Osteoporotic Rats. Int. J. Biol. Sci. *12*, 836–849. https://doi.org/10.7150/ijbs.14809.
21. Wang, L., Pan, Y., Liu, M., Sun, J., Yun, L., Tu, P., Wu, C., Yu, Z., Han, Z., Li, M., et al. (2023). Wen-Shen-Tong-Luo-Zhi-Tong Decoction regulates bone-fat balance in osteoporosis by adipocyte-derived exosomes. Pharm. Biol. *61*, 568–580. https://doi.org/10.1080/13880209.2023.2190773.
22. Agbu, P., and Carthew, R.W. (2021). MicroRNA-mediated regulation of glucose and lipid metabolism. Nat. Rev. Mol. Cell Biol. *22*, 425–438. https://doi.org/10.1038/s41580-021-00354-w.
23. Fabian, M.R., Sonenberg, N., and Filipowicz, W. (2010). Regulation of mRNA translation and stability by microRNAs. Annu. Rev. Biochem. *79*, 351–379. https://doi.org/10.1146/annurev-biochem-060308-103103.
24. Krol, J., Loedige, I., and Filipowicz, W. (2010). The widespread regulation of microRNA biogenesis, function and decay. Nat. Rev. Genet. *11*, 597–610. https://doi.org/10.1038/nrg2843.
25. Li, D., Liu, J., Guo, B., Liang, C., Dang, L., Lu, C., He, X., Cheung, H.Y., Xu, L., Lu, C., et al. (2016). Osteoclast-derived exosomal miR-214-3p inhibits osteoblastic bone formation. Nat. Commun. *7*, 10872. https://doi.org/10.1038/ncomms10872.
26. Zhu, S., Yao, F., Qiu, H., Zhang, G., Xu, H., and Xu, J. (2018). Coupling factors and exosomal packaging microRNAs involved in the regulation of bone remodelling. Biol. Rev. Camb. Phil. Soc. *93*, 469–480. https://doi.org/10.1111/brv.12353.
27. Yang, X., Yang, J., Lei, P., and Wen, T. (2019). LncRNA MALAT1 shuttled by bone marrow-derived mesenchymal stem cells-secreted exosomes alleviates osteoporosis through mediating microRNA-34c/SATB2 axis. Aging (Albany NY) *11*, 8777–8791. https://doi.org/10.18632/aging.102264.
28. Cui, Y., Guo, Y., Kong, L., Shi, J., Liu, P., Li, R., Geng, Y., Gao, W., Zhang, Z., and Fu, D. (2022). A bone-targeted engineered exosome platform delivering siRNA to treat osteoporosis. Bioact. Mater. *10*, 207–221. https://doi.org/10.1016/j.bioactmat.2021.09.015.
29. Cui, Y., Li, Z., Guo, Y., Qi, X., Yang, Y., Jia, X., Li, R., Shi, J., Gao, W., Ren, Z., et al. (2022). Bioinspired Nanovesicles Convert the Skeletal Endothelium-Associated Secretory Phenotype to Treat Osteoporosis. ACS Nano *16*, 11076–11091. https://doi.org/10.1021/acsnano.2c03781.
30. Li, J., Zhang, R., Du, Y., Liu, G., Dong, Y., Zheng, M., Cui, W., Jia, P., and Xu, Y. (2023). Osteophilic and Dual-Regulated Alendronate-Gene Lipoplexes for Reversing Bone Loss. Small *19*, e2303456. https://doi.org/10.1002/smll.202303456.
31. Ko, J.Y., Chuang, P.C., Ke, H.J., Chen, Y.S., Sun, Y.C., and Wang, F.S. (2015). MicroRNA-29a mitigates glucocorticoid induction of bone loss and fatty marrow by rescuing Runx2 acetylation. Bone *81*, 80–88. https://doi.org/10.1016/j.bone.2015.06.022.
32. Böhm, C., Derer, A., Axmann, R., Hillienhoff, U., Zaiss, M.M., Luther, J., Zech, C., Stock, M.,

Scholtysek, C., Engelke, K., et al. (2012). RSK2 protects mice against TNF-induced bone loss. J. Cell Sci. *125*, 2160–2171. https://doi.org/10.1242/jcs.096008.

33. Haxaire, C., Hakobyan, N., Pannellini, T., Carballo, C., McIlwain, D., Mak, T.W., Rodeo, S., Acharya, S., Li, D., Szymonifka, J., et al. (2018). Blood-induced bone loss in murine hemophilic arthropathy is prevented by blocking the iRhom2/ADAM17/TNF-α pathway. Blood *132*, 1064–1074. https://doi.org/10.1182/blood-2017-12-820571.
34. Wijbrandts, C.A., Klaasen, R., Dijkgraaf, M.G., Gerlag, D.M., van Eck-Smit, B.L., and Tak, P.P. (2009). Bone mineral density in rheumatoid arthritis patients 1 year after adalimumab therapy: arrest of bone loss. Ann. Rheum. Dis. *68*, 373–376. https://doi.org/10.1136/ard.2008.091611.
35. Esatbeyoglu, T., Huebbe, P., Ernst, I.M., Chin, D., Wagner, A.E., and Rimbach, G. (2012). Curcumin–from molecule to biological function. Angew Chem. Int. Ed. Engl. *51*, 5308–5332. https://doi.org/10.1002/anie.201107724.
36. Fan, D., Lu, J., Yu, N., Xie, Y., and Zhen, L. (2022). Curcumin Prevents Diabetic Osteoporosis through Promoting Osteogenesis and Angiogenesis Coupling via NF-κB Signaling. Evid Based Complement Alternat Med *2022*, 4974343. https://doi.org/10.1155/2022/4974343.
37. Chen, Z., Xue, J., Shen, T., Mu, S., and Fu, Q. (2016). Curcumin alleviates glucocorticoid-induced osteoporosis through the regulation of the Wnt signaling pathway. Int. J. Mol. Med. *37*, 329–338. https://doi.org/10.3892/ijmm.2015.2432.
38. Yang, X., Kuang, Z., Yang, X., Hu, X., Luo, P., Lai, Q., Zhang, B., Zhang, X., and Wei, Y. (2023). Facile synthesis of curcumin-containing poly(amidoamine) dendrimers as pH-responsive delivery system for osteoporosis treatment. Colloids Surf. B Biointerfaces *222*, 113029. https://doi.org/10.1016/j.colsurfb.2022.113029.
39. Heo, D.N., Ko, W.K., Moon, H.J., Kim, H.J., Lee, S.J., Lee, J.B., Bae, M.S., Yi, J.K., Hwang, Y.S., Bang, J.B., et al. (2014). Inhibition of osteoclast differentiation by gold nanoparticles functionalized with cyclodextrin curcumin complexes. ACS Nano *8*, 12049–12062. https://doi.org/10.1021/nn504329u.
40. Chen, Z., Xue, J., Shen, T., Ba, G., Yu, D., and Fu, Q. (2016). Curcumin alleviates glucocorticoid-induced osteoporosis by protecting osteoblasts from apoptosis in vivo and in vitro. Clin. Exp. Pharmacol. Physiol. *43*, 268–276. https://doi.org/10.1111/1440-1681.12513.
41. Zarrin, P., Dehghani Ashkezari, M., and Seifati, S.M. (2021). Liposomal Form of L-Dopa and SH-Sy5y Cell-Derived Exosomes Modulate the Tyrosine Hydroxylase/Dopamine Receptor D2 Signaling Pathway in Parkinson's Rat Models. J. Mol. Neurosci. *71*, 2583–2592. https://doi.org/10.1007/s12031-021-01853-3.
42. Safakheil, M., and Safakheil, H. (2020). The Effect of Exosomes Derived from Bone Marrow Stem Cells in Combination with Rosuvastatin on Functional Recovery and Neuroprotection in Rats After Ischemic Stroke. J. Mol. Neurosci. *70*, 724–737. https://doi.org/10.1007/s12031-020-01483-1.
43. Liu, Y., Song, B., Wei, Y., Chen, F., Chi, Y., Fan, H., Liu, N., Li, Z., Han, Z., and Ma, F. (2018). Exosomes from mesenchymal stromal cells enhance imatinib-induced apoptosis in human leukemia cells via activation of caspase signaling pathway. Cytotherapy *20*, 181–188. https://doi.org/10.1016/j.jcyt.2017.11.006.

STAR★METHODS

KEY RESOURCES TABLE

REAGENT or RESOURCE	SOURCE	IDENTIFIER
Antibodies		
Anti-TSG101 antibody	Abcam	Cat# ab125011, RRID: AB_10974262
Anti-CD63 antibody	Abcam	AB_216130
Anti-CD9 antibody	Abcam	Cat# ab92726, RRID: AB_10561589
Anti-Calnexin antibody	Cell Signaling Technology	Cat# 2679, RRID: AB_2228381
Anti-TNF antibody	Abcam	Cat# ab183218, RRID: AB_2889388
Anti-GAPDH antibody	Abcam	Cat# ab8245, RRID: AB_2107448
HRP-labeled Goat Anti-Rabbit IgG (H+L)	Beyotime	Cat# A0208, RRID: AB_2892644
Horseradish-labeled goat anti-mouse IgG (H+L) antibody	Beyotime	Cat# A0216, RRID: AB_2860575
Chemicals, peptides, and recombinant proteins		
Recombinant Mouse M-CSF	Novoprotein	Cat. No.: CB34
Recombinant Mouse RANK L	Novoprotein	Cat. No.: CJ94
mimic control	Ribobio	miR1N0000001-1-5
miR-3p-975_4191 mimic	Ribobio	miR1220607031829
micrOFF inhibitor NC	Ribobio	miR2N0000001-1-5
micrOFFTM PC-3p-975_4191 inhibitor	Ribobio	miR2240116015227
β-glycerol phosphate	Sigma	G9422
Ascorbate-2-phosphate	Sigma	A4544
3-isobutyl-1-methylxanthine	Sigma	I5879250MG
Insulin	Sigma	91077C-250MG
Trypsin	Solarbio	T1320
Dexamethasone	Sigma	D4902
Alizarin Red S Solution	Sigma-Aldrich	T201112D501
Critical commercial assays		
HiScript® II Q RT SuperMix for qPCR (+g DNA wiper)	Vazyme	R223-01
ChamQ Universal SYBR qPCR Master Mix	Vazyme	Q711-02/03
Double luciferase reporter gene assay	Biossci	N/A
Experimental models: Cell lines		
Human: HMEC-1	The Second Xiangya Hospital, Central South University	N/A
Mouse: BMSC	C57BL/6J mice, Hunan Slaughter Jingda Laboratory Animal Co., Ltd	N/A
Experimental models: Organisms/strains		
C57BL/6J mice	Hunan Slaughter Jingda Laboratory Animal Co., Ltd	N/A
Oligonucleotides		
Primers for qRT-PCR, see Table S2.	This paper	N/A
Deposited data		
miRNA-sequencing raw and processed data	NCBI-SRA	Accession numbers: PRJNA1086715

(*Continued on next page*)

Continued

REAGENT or RESOURCE	SOURCE	IDENTIFIER
Software and algorithms		
GraphPad Prism 8	GraphPad	N/A
ImageJ	NIH	https://imagej.nih.gov/ij/
NRecon v1.6	Bioz, Palo Alto	https://www.microphotonics.com/products/micro-ct/nrecon-reconstruction-software/
CT Analyser v1.9	Bruker microCT	https://www.bruker.com
mCT Volume v2.0	Bruker microCT	https://www.bruker.com

RESOURCE AVAILABILITY

Lead contact

The relevant experimental reagents, experimental methods, and related data of this study can be obtained by contacting Qiong Lu (christy_luq@csu.edu.cn).

Materials availability

The study did not generate unique reagents.

Data and code availability

- MiRNA-sequencing raw and processed data have been deposited to NCBI Sequence ReadArchive (SRA) and are publicly available as of the date of publication. Accession numbers are PRJNA1086715.
- This paper does not report original code.
- Any additional data and information needed to analyze the data in this paper can be obtained from the lead contact upon request.

EXPERIMENTAL MODEL AND STUDY PARTICIPANT DETAILS

Statement of ethics

The animal experimental procedures were carried out in accordance with the regulations of the Institutional Animal Care and Use Committee of the Second Xiangya Hospital of Central South University (Changsha, Hunan, China).

Animal models

Twelve 15-month-old male C57BL/6 mice were purchased from Hunan Slaughter Jingda Laboratory Animal Co., Ltd. The mice were randomly assigned to two groups: the EC-EXO-treated group (EC-EXO group, n=6) and the PBS-treated group (control group, n=6). The mice were injected with EC-EXOs through the tail vein for 4 weeks. Eighteen 8-week-old female C57BL/6 mice were also purchased from Hunan Slaughter Jingda Experimental Animal Co., Ltd. Animal models of postmenopausal osteoporosis were established by surgical bilateral ovariectomy (OVX). The mice were randomly assigned to three groups: the EC-EXO-treated bilateral OVX group (OVX-EC-EXO group, n=6), PBS-treated bilateral OVX group (OVX-PBS, n=6) and PBS-treated sham-operated group (sham-PBS, n=6). The mice were injected with EC-EXOs through the tail vein for 4 weeks.

Surgical bilateral OVX or sham operation was performed in an aseptic environment. Linear incisions of 10 mm were made bilaterally in the skin on the lumbar side in both the OVX and sham-operation groups. After blunt dissection to expose the muscle and peritoneum, OVX was performed in the OVX group, and the bilateral ovaries were identified and placed back into the abdominal cavity in the sham-operated group. The abdominal incisions in both groups were carefully sutured.

METHOD DETAILS

Isolation of mouse BMSCs

C57BL/6J mice were anesthetized with pentobarbital and then sacrificed. The tibias and femurs of the mice were separated, and the ends of the tibias and femurs were cut. The bone marrow was flushed out with a 10 ml syringe with a 25-gauge needle filled with 10 ml of 1× PBS. The cell suspensions were centrifuged at 700 × g for 5 minutes at 4°C, and the cells were resuspended in 500 μl of 1× PBS. Then, the cell suspensions were incubated with anti-Sca-1-PE (BioLegend, USA), anti-CD29-FITC (BioLegend, USA), anti-CD45-PerCP (BioLegend, USA), and anti-CD11b-PerCP (BioLegend, USA) antibodies for 30 minutes at 4°C. The mouse BMSCs ($Sca\text{-}1^{+}CD29^{+}CD45^{-}CD11b^{-}$) were sorted by fluorescence-activated cell sorting (FACS) with a FACSAria (BD Biosciences, USA) and cultured with α-MEM culture medium (Cellmax,

China) with 10% fetal bovine serum (FBS) and 1% streptomycin (Gibco, USA) and penicillin (Gibco, USA) at 37°C in a humidified atmosphere of 5% CO_2.

Isolation and characterization of exosomes

HMEC-1 cells were cultured with MCDB131 medium (Procell, China) containing 10% FBS and 1% penicillin–streptomycin until they reached 60-70% confluence. The cell supernatant was discarded, and then the pellet was washed with 1× PBS and resuspended with exosome-removed FBS. Cell supernatants were collected at 24 h intervals according to cell density. Briefly, the supernatant samples were centrifuged at 2000 × g for 10 minutes to remove cellular debris and then centrifuged at 10,000 × g for 30 minutes at 4°C. The HMEC-1 exosomes were isolated by ultracentrifugation (Beckman, USA) at 10,0000 ×g for 70 min and cleaned with 1× PBS. The isolated exosomes were immediately used for follow-up experiments or stored at -80°C.

Transmission electron microscopy (TEM)

For TEM, 15 μl of exosome suspension was adsorbed onto a copper grid and left to stand for 1 minute. The exosome sample on the copper grid was blotted with filter paper and stained with 2% uranyl acetate staining solution for 1 minute at room temperature. The exosome samples were blotted dry, and the finished stained samples were placed under a lamp for 10 min. Finally, images were obtained with a transmission electron microscope (Tecnai, USA).

Nanoparticle tracking analysis (NTA)

NTA (NanoSight NS300, Britain) was used to detect the distribution and particle size of exosomes. The sample cell was washed with ultrapure water to prevent residual particles from affecting the results. After calibration of the instrument with polystyrene microspheres (100 nm), the sample cell was washed with PBS. The samples were diluted with PBS and injected for analysis.

Exosome labeling and coculture with BMSCs

Diluent C and PKH67 (Sigma, USA) were added according to the volume of exosomes, thoroughly mixed and incubated at room temperature for 5 min. Then, 1% BSA was added to terminate staining for 1 min, the volume of the mixture was increased to 20 ml with 1% BSA, the samples were centrifuged at 120,000 × g with an ultra-high-speed centrifuge (Beckman, USA) for 60 min, and the supernatant was discarded. The PKH67-Exo precipitate was dissolved in 1× PBS and added to α-MEM culture medium containing exosome-free FBS. BMSCs were incubated with this culture medium for 48 h at 37°C. After 48 h, the medium was discarded, the cells were fixed with 4% paraformaldehyde, and the BMSCs were washed with 1× PBS three times. The cells were treated with 0.1% Triton X-100 for 5 min and sealed with a blocker containing DAPI. The cells were observed and photographed with a laser confocal microscope (Leica, Germany).

Western blot analysis

Cells were collected and lysed with radioimmunoprecipitation assay (RIPA) lysis buffer (Beyotime, China) at 4°C for 30 min. The cell lysates were centrifuged at 10,000 × g for 30 min at 4°C. The cell proteins were extracted, and the supernatants were collected. The protein concentrations of the cell supernatants were quantified using a Pierce BCA Protein Assay Kit (Thermo Fisher Scientific, USA). Equal amounts of cell lysates were loaded and separated by SDS–PAGE and then blotted onto PVDF membranes. The membranes were incubated with primary antibodies against CD9 (Abcam, 1:1000), CD63 (Abcam, 1:1000), TSG101 (Abcam, 1:1000) and calnexin (Cell Signaling Technology, 1:1000) overnight at 4°C. The next day, the membranes were incubated with anti-mouse/rabbit secondary antibodies (Beyotime, China) for 1 h at room temperature. Enhanced chemiluminescence (ECL) solution (Share-bio, China) and Image Studio software (Thermo Fisher Scientific, USA) were used to visualize the blot bands.

Adipogenic differentiation

For adipogenic differentiation of BMSCs, BMSCs were cultured in adipogenic differentiation medium (Sigma, USA) consisting of α-MEM supplemented with 15% FBS, 1% penicillin–streptomycin, 1 nM dexamethasone, 0.05 mM vitamin C, 0.5 mM isobutyl methylxanthine (IBMX), 50 μM indomethacin and 5 μg/ml insulin for 14 days when the cell confluence reached 90%–100%. The medium was replaced every 3 days.

Osteogenic differentiation

For osteogenic differentiation of BMSCs, BMSCs were cultured in osteogenic differentiation medium (Sigma, USA) consisting of α-MEM supplemented with 15% FBS, 1% penicillin–streptomycin, 0.1 nM dexamethasone, 0.05 mM vitamin C and 10 mM b-glycerophosphate for 21 days when the cell confluence reached 60%–70%. The medium was replaced every 3 days.

Oil red O staining and quantitative analysis

Lipid droplet formation in BMSCs was detected by Oil red O staining. Briefly, the cells were washed with 1× PBS three times and then fixed with 4% paraformaldehyde (Langeco Technology, China) at room temperature for 30 min after adipogenesis. The fixed cells were washed with 1× PBS again and stained with Oil red O dye liquor (Starfish Biotechnology, China) for 30 min. The cells were photographed under an inverted

optical microscope (Olympus, Japan). The adipocytes exhibited red oil droplets under a microscope. For quantification of the formation of lipid droplets in BMSCs, the cells were incubated with isopropyl alcohol for 10 min. After elution of the lipid droplets, the absorbance of the eluted lipid droplets was measured at 510 nm using a microplate reader (Thermo Fisher Scientific, USA).

Alizarin red staining and quantitative analysis

Osteogenic differentiation of BMSCs was detected by Alizarin red staining. After osteogenesis, the cells were washed three times with 1× PBS and fixed with 4% polyformaldehyde for 30 min. Then, the cells were washed with 1× PBS again and incubated with Alizarin red staining solution for 5 min. The cells were rinsed 3 times with 1× PBS, and representative photographs were taken. For quantification of the mineralization degree of BMSCs, the cells were incubated in the presence of 10% cetylpyridinium chloride (Sigma, USA) for 15 min. The staining of calcium nodules was observed under an inverted microscope. The absorbance of the eluted calcium nodules was measured at 562 nm using a microplate reader.

Quantitative real-time PCR (qRT–PCR) analysis

Total RNA was extracted with TRIzol Reagent (TaKaRa, Japan) and qualified with a NanoDrop spectrophotometer. (Thermo Fisher Scientific, USA). The extracted RNA was reverse-transcribed into cDNA using PrimeScript RT Master Mix. The conditions were as follows: 95°C for 30 s, 40 cycles at 95°C for 10 s and 60°C for 30 s, and dissolving at 95°C for 15 s, 60°C for 60 s and 95°C for 15 s. qRT–PCR was performed using Power SYBR Green PCR Master Mix to measure the expression of target genes. β-Actin was used as the endogenous control to normalize the expression of genes. Relative gene expression was calculated, normalized, and assessed by the $2^{-\Delta\Delta CT}$ approach. All samples were tested three times. The primers used for qRT–PCR amplification are listed in Table S2.

Animal model and grouping

Twelve 15-month-old male C57BL/6 mice were purchased from Hunan Slaughter Jingda Laboratory Animal Co., Ltd. The mice were randomly assigned to two groups: the EC-EXO-treated group (EC-EXO group, n=6) and the PBS-treated group (control group, n=6). The mice were injected with EC-EXOs through the tail vein for 4 weeks. Eighteen 8-week-old female C57BL/6 mice were also purchased from Hunan Slaughter Jingda Experimental Animal Co., Ltd. Animal models of postmenopausal osteoporosis were established by surgical bilateral ovariectomy (OVX). The mice were randomly assigned to three groups: the EC-EXO-treated bilateral OVX group (OVX-EC-EXO group, n=6), PBS-treated bilateral OVX group (OVX-PBS, n=6) and PBS-treated sham-operated group (sham-PBS, n=6). The mice were injected with EC-EXOs through the tail vein for 4 weeks.

Surgical bilateral OVX or sham operation was performed in an aseptic environment. Linear incisions of 10 mm were made bilaterally in the skin on the lumbar side in both the OVX and sham-operation groups. After blunt dissection to expose the muscle and peritoneum, OVX was performed in the OVX group, and the bilateral ovaries were identified and placed back into the abdominal cavity in the sham-operated group. The abdominal incisions in both groups were carefully sutured. The animal experimental procedures were carried out in accordance with the regulations of the Institutional Animal Care and Use Committee of the Second Xiangya Hospital of Central South University (Changsha, Hunan, China).

Micro-CT analysis

Samples were scanned using a micro-CT scanner (Bruker micro-CT, USA). All images were manipulated manually to separate cancellous and cortical bone and preserve their morphology. Scans were repeated three times, with bone microstructural parameters acquired from the same region of interest (ROI) for each group. Structural parameters of the ROI, including trabecular bone volume/tissue volume (BV/TV), trabecular number (Tb.N), trabecular separation (Tb.Sp) and trabecular thickness (Tb.Th) were analyzed with image reconstruction software (NRecon, USA), data analysis software (Bruker micro-CT, USA), and 3-dimensional model visualization software (Bruker micro-CT, USA).

Histochemistry and immunocytochemistry

After fixation and decalcification of the femur, the femur was dehydrated and paraffin-embedded. Paraffin blocks of femur were cut into 5 μm thick sections, applied to slides and rehydrated step by step with 100%, 95%, 70% and 50% alcohol solutions. The slides were stained using a TRAP staining kit (Sigma–Aldrich, USA) and hematoxylin and eosin (HE) (Sigma–Aldrich, USA) for immunohistochemical analysis. The stained slides were dehydrated, mounted for observation under a phase contrast microscope (Q500MC, Leica Microsystems, Germany) and analyzed using specialized image analysis software (ImageJ).

Microarray analysis

RNA was extracted from the EC-EXO treatment group and control group and used for miRNA microarray analysis. The experimental procedures were performed according to standard protocols provided by Illumina, including library preparation and sequencing. TruSeq Small RNA Sample Prep Kits (Illumina, San Diego, USA) were used to prepare the small RNA sequencing library. After the library was prepared, it was sequenced with an Illumina HiSeq 2000/2500 instrument, and the sequencing read length was 1×50 bp. Raw reads were subjected to an in-house program, ACGT101-miR (LC Sciences, Houston, Texas, USA), to remove adapter dimers, junk, low complexity, common RNA families (rRNA, tRNA, snRNA, snoRNA), and repeats. Subsequently, unique sequences with a length of 18∼26 nucleotides were mapped to specific

species precursors in miRBase 22.0 by BLAST search to identify known miRNAs and 3p- and 5p-derived miRNAs. Both length variations at both the 3′ and 5′ ends and one mismatch inside the sequence were allowed in the alignment. The unique sequences mapping to specific species of mature miRNAs in hairpin arms were identified as known miRNAs. The unique sequences mapping to the other arm of a known specific species precursor hairpin opposite to the annotated mature miRNA-containing arm were considered to be 5p- or 3p-derived miRNA candidates. The remaining sequences were mapped to other selected species precursors (with the exclusion of specific species) in miRBase 22.0 by BLAST search, and the mapped pre-miRNAs were further BLASTed against the specific species genomes to determine their genomic locations. The above two were defined as known miRNAs. The unmapped sequences were BLASTed against the specific genomes, and the hairpin RNA structures containing sequences were predicated from the flank 80 nt sequences using RNAfold software (http://rna.tbi.univie.ac.at/cgi-bin/RNAfold.cgi). The criteria for secondary structure prediction were: (1) number of nucleotides in one bulge in stem ($\leq$12); (2) number of base pairs in the stem region of the predicted hairpin ($\geq$16) (3) cutoff of free energy (kCal/mol $\leq$-15) (4) length of hairpin (up and down stems + terminal loop $\geq$50) (5) length of hairpin loop ($\leq$20). (6) number of nucleotides in one bulge in mature region ($\leq$8) (7) number of biased errors in one bulge in mature region ($\leq$4) (8) number of biased bulges in mature region ($\leq$2) (9) number of errors in mature region ($\leq$7) (10) number of base pairs in the mature region of the predicted hairpin ($\geq$12) (11) percent of mature stems ($\geq$80). Differentially expressed miRNAs were screened with thresholds of a p value < 0.05 and a | log fold change | > 2. Heatmaps of the differentially expressed miRNAs were subsequently plotted. TargetScan (v5.0) and miRanda (v3.3a) were used to predict the target genes of the miRNAs with significant differences. Several databases were employed, including miRBase (miRNAs and premiRNAs; ftp://mirbase.org/pub/mirbase/CURRENT/), RFam (a collection of many common noncoding RNA families except miRNAs; http://rfam.janelia.org), Repbase (a collection of prototypic sequences representing repetitive DNA from different eukaryotic species; http://www.girinst.org/repbase), Ensembl (genomic data and mRNA; ftp://ftp.ensembl.org/pub/release-101/fasta/homo_sapiens/dna/), the Kyoto Encyclopedia of Genes and Genomes (KEGG) (pathways; http://www.genome.jp/kegg), and the Gene Ontology database (ftp://ftp.ncbi.nih.gov/gene/DATA/gene2go.gz).

Cell transfection

MiRNA transfection was performed when the cell confluence reached 60%–80%. The medium of BMSCs was replaced with fresh α-MEM culture medium two hours before transfection. The mimic negative control and miR-3p-975_4191 mimic (RiboBio, China) was dissolved in Opti-MEM (Gibco, USA) separately. Each solution was combined with the transfection reagent (Neofect, China) according to the manufacturer's protocol. The resulting transfection mixture was then gently mixed and allowed to stand for 15∼30 minutes. The expression level of miR-3p-975_4191 was detected after incubation for 48 h.

Cell counting kit-8 (CCK-8) assay

Cells cultured in 96-well plates were treated with different concentrations of curcumin for 0, 24 and 48 hours. CCK-8 reagent was added to the medium (1:100), and the cells were incubated for another 4 hours. Cell proliferation was assessed by measuring the optical density (OD) at 450 nm using a microplate reader (Beyotime, China) according to the manufacturer's instructions.

QUANTIFICATION AND STATISTICAL ANALYSIS

All data were presented as mean ± SEM from at least three replicates for each experiment. The analyses were performed using GraphPad Prism 8 (GraphPad Software, USA). Comparison between two groups was conducted using Student's unpaired t test. One-way analysis of variance (ANOVA) with Tukey's multiple comparison tests was used to analyze the statistical significance of differences among more than two groups. A value of $p < 0.05$ was considered to indicate significance, and values of $p < 0.01$ and < 0.001 were considered to indicate extreme significance.